

1 **The roles of charge exchange and dissociation in**
2 **spreading Saturn's neutral clouds**

B. L. Fleshman, P. A. Delamere, F. Bagenal, T. Cassidy

arXiv:1204.0979v1 [physics.space-ph] 4 Apr 2012

F. Bagenal, Laboratory for Atmospheric and Space Physics, University of Colorado Boulder,
Colorado 80309-0391

T. Cassidy, Laboratory for Atmospheric and Space Physics, University of Colorado Boulder,
Colorado 80309-0391

P. A. Delamere, Laboratory for Atmospheric and Space Physics, University of Colorado Boul-
der, Colorado 80309-0391

B. L. Fleshman, Homer L. Dodge Department of Physics and Astronomy, The University of
Oklahoma, 440 W. Brooks St., Norman, OK 73019, USA. (fleshman@nhn.ou.edu)

3 **Abstract.** Neutrals sourced directly from Enceladus's plumes are initially
4 confined to a dense neutral torus in Enceladus's orbit around Saturn. This
5 neutral torus is redistributed by charge exchange, impact/photodissociation,
6 and neutral-neutral collisions to produce Saturn's neutral clouds. Here we
7 consider the former processes in greater detail than in previous studies. In
8 the case of dissociation, models have assumed that OH is produced with a
9 single speed of 1 km s^{-1} , whereas laboratory measurements suggest a range
10 of speeds between 1 and 1.6 km s^{-1} . We show that the high-speed case in-
11 creases dissociation's range of influence from 9 to $15 R_S$. For charge exchange,
12 we present a new modeling approach, where the ions are followed within a
13 neutral background, whereas neutral cloud models are conventionally con-
14 structed from the neutrals' point of view. This approach allows us to com-
15 ment on the significance of the ions' gyrophase at the moment charge exchange
16 occurs. Accounting for gyrophase: (1) has no consequence on the H_2O cloud;
17 (2) doubles the local density of OH at the orbit of Enceladus; and (3) de-
18 creases the oxygen densities at Enceladus's orbit by less than 10%. Finally,
19 we consider velocity-dependent, as well as species-dependent cross sections
20 and find that the oxygen cloud produced from charge exchange is spread out
21 more than H_2O , whereas the OH cloud is the most confined.

1. Introduction

22 The Enceladus plumes directly produce a dense H₂O torus centered on Enceladus's
23 orbit, within which charge exchange and dissociation subsequently produce neutrals that
24 either feed Saturn's extended neutral clouds, collide (absorb) with Saturn and its rings,
25 or leave the system altogether on escape orbits. This paper is a report on the results
26 of a sensitivity study of low-velocity charge exchange and dissociation within the neutral
27 torus.

28 Several decades before Cassini arrived at Saturn and the Enceladus water plumes were
29 discovered [*Hansen et al.*, 2006], neutral hydrogen was observed in Saturn's magne-
30 sphere, both from Earth [*Weiser et al.*, 1977] and from Voyagers 1 and 2 [*Shemansky and*
31 *Hall*, 1992]. Hydroxyl was later discovered by *Shemansky et al.* [1993] with HST, and
32 more recently, *Esposito et al.* [2005] detected atomic oxygen. These observations collec-
33 tively hinted at the presence of a source of water, and models predicted its location to be
34 near the orbit of Enceladus (c.f., *Jurac et al.* [2002]).

35 After identifying the Enceladus plumes as the dominant source of the water-group
36 neutrals (O, OH, H₂O)—and indeed the co-rotating plasma itself via electron impact
37 and photoionization [*Young et al.*, 2005; *Sittler et al.*, 2005, 2008]—researchers have been
38 attempting to understand how neutrals are transported from Enceladus to 20 Saturn
39 radii ($R_S = 6 \times 10^9$ cm) and beyond, as observed by *Shemansky et al.* [1993], *Esposito*
40 *et al.* [2005], and most recently by *Melin et al.* [2009]. Early on, *Jurac et al.* [2002]
41 mentioned the role of charge exchange in this inflation process. *Johnson et al.* [2006] later
42 showed that if magnetospheric plasma is slowed sufficiently with respect to neutrals in

43 the Enceladus torus, then charge exchange produces a sufficient number of particles with
44 velocities capable of spreading the dense H₂O Enceladus torus into the cloud observed by
45 *Shemansky et al.* [1993].

46 *Farmer* [2009] pointed out the importance of dipole–dipole interactions in collisions
47 involving H₂O molecules. She showed that collisions inside the dense Enceladus torus
48 (parameterized by macroscopic viscosity) are alone sufficient for the creation of the ex-
49 tended component of Saturn’s neutral cloud. *Cassidy and Johnson* [2010] later argued
50 that *Farmer*’s fluid treatment is inappropriate for neutral–neutral collisions in the Ence-
51 ladus torus, where the mean free path is on the order of the torus size itself. Instead,
52 *Cassidy and Johnson* [2010] approached the problem with a direct simulation Monte Carlo
53 (DSMC) model. Their model self-consistently included losses due to charge exchange, dis-
54 sociation, and ionization, whereas *Farmer* [2009] accounted for losses to charge exchange
55 and ionization by evolving the neutral cloud for the time scales (months to a few years)
56 found in *Sittler et al.* [2008]. Both studies agree that neutral–neutral collisions are neces-
57 sary for the inflation of Saturn’s neutral cloud.

58 Collisions between neutrals occur at a rate proportional to the square of the neutral
59 density. Thus, where neutral densities peak near the orbit of Enceladus, neutral–neutral
60 collisions occur more often than either charge exchange or dissociation, whereas near 6
61 R_S, neutral densities drop and all three processes become comparable (see Fig. 3, *Cassidy*
62 *and Johnson* [2010]). Models involving neutral collisions have recently been validated
63 with Herschel observations by *Hartogh et al.* [2011], who attribute a warm and broadened
64 Enceladus torus to heating via neutral–neutral collisions; the effect of these interactions
65 should therefore be included in any attempt to fully model Saturn’s neutral clouds. Nev-

66 ertheless, several first-order conclusions can be drawn by revisiting charge exchange and
 67 dissociation.

68 Previous neutral cloud models approach charge exchange from the neutrals' point of
 69 view, whereas we follow the ion along its trajectory, thus allowing us to identify the
 70 gyrophase at which an ion undergoes charge exchange. We find that including the phase
 71 dependence doubles OH densities at the orbit of Enceladus, decreases oxygen density by
 72 $\lesssim 10\%$, and has no effect on H₂O (section 3.1). Also, the velocity-dependence of charge
 73 exchange varies by species. Previous studies (*e.g.*, *Johnson et al.* [2006]; *Cassidy and*
 74 *Johnson* [2010]) have considered velocity-dependence, but have used a single cross section
 75 to represent all charge exchanges. We show in section 3.1 that symmetric reactions such as
 76 $\text{H}_2\text{O} + \text{H}_2\text{O}^+ \rightarrow \text{H}_2\text{O}^+ + \text{H}_2\text{O}^*$ (the asterisk identifies a neutral released with the speed of
 77 the reacting ion) tend to distribute neutrals closer to Saturn, while asymmetric exchanges
 78 such as $\text{H}_2\text{O} + \text{O}^+ \rightarrow \text{H}_2\text{O}^+ + \text{O}^*$ populate a more extended cloud, with less absorption
 79 on Saturn.

80 With regard to dissociation, OH produced by impact/photodissociation of H₂O has pre-
 81 viously been modeled with an initial speed of 1 km s^{-1} [*Jurac and Richardson*, 2005; *Cas-*
 82 *sidy and Johnson*, 2010], whereas recent laboratory measurements span 1 to 1.6 km s^{-1} ,
 83 depending on the molecule's internal energy [*Wu and Chen*, 1993; *Makarov et al.*, 2004].
 84 We model this parameter space and find that, relative to charge exchange, most OH found
 85 inside $9 R_S$ is produced by dissociation when OH is dissociated from H₂O at 1 km s^{-1} ,
 86 with that location extended to $15 R_S$ when OH is dissociated from H₂O at 1.6 km s^{-1}
 87 instead.

88 This paper is organized as follows. The model for the production of neutrals via dis-
89 sociation and three illustrative charge exchanges is explained in section 2. Our results
90 are found in section 3, followed by a discussion in section 4. The important points are
91 summarized in section 5.

2. Model

92 We begin with a few words on nomenclature. The neutral torus in this paper pertains
93 to the primary neutral torus (not plasma torus) supplied directly by Enceladus's plumes.
94 The neutral clouds refer to the secondary neutrals produced from charge exchange and
95 dissociation in the neutral torus.

96 The production of Saturn's neutral cloud is modeled in two steps. We first construct
97 a dense H₂O torus from a plume positioned at Enceladus's south pole with specifications
98 based on several Cassini Enceladus flybys (*Smith et al.* [2010]; see also *Smith et al.* [2004],
99 *Smith* [2006], and *Smith et al.* [2007]). Secondary neutrals are then produced from the
100 primary neutral torus by charge exchange and dissociation, some of which remain grav-
101 itationally bound to Saturn and form the neutral clouds. On the basis that they spend
102 most of the time outside the neutral torus and plasma sheet, we assume their lifetimes to
103 be determined solely by photo-processes, though in section 3.3, we consider the effects of
104 charge exchange and electron impact.

2.1. Neutral torus model

105 The neutral torus and Enceladus plume models are described in the following subsec-
106 tions.

2.1.1. Enceladus H₂O torus

108 Our aim is to study the effects of several important reactions occurring in Enceladus's
 109 orbit. The primary neutral torus, fed directly by Enceladus, is produced in the model by
 110 evolving water molecules released from Enceladus into a dense neutral torus centered on
 111 Enceladus's orbit ($3.95 R_S$). The assumption is that all H_2O is initially produced by a
 112 single plume at Enceladus's south pole. In reality, more than one plume has been observed
 113 [*Porco et al.*, 2006], and researchers such as *Saur et al.* [2008] and *Smith et al.* [2010] have
 114 studied their signature on flyby observations. For our purposes, the detailed influence
 115 of multiple plumes can be neglected. The plume particles' radial speed distribution is
 116 prescribed as a one-dimensional Maxwellian with temperature $T = 180$ K [*Spencer et al.*,
 117 2006; *Hansen et al.*, 2006]:

$$f(v) = \left(\frac{m_{H_2O}}{2\pi kT}\right)^{1/2} \exp\left[-\frac{m_{H_2O}}{2kT}(v - v_{\text{bulk}})^2\right], \quad (1)$$

118 where v_{bulk} is the bulk speed, equal to 720 m s^{-1} , $1.8\times$ the thermal speed estimated by
 119 *Smith et al.* [2010] ($v_{\text{therm}} = \sqrt{2kT/m_{H_2O}} = 400 \text{ m s}^{-1}$). Additionally, a raised cosine
 120 distribution is used to determine where the molecules are released:

$$g(\theta) = \begin{cases} \frac{1}{\theta_0} \left[1 + \cos\left(\frac{\theta}{\theta_0}\pi\right)\right] & \text{if } \theta < \theta_0 = 30^\circ \\ 0 & \text{otherwise.} \end{cases} \quad (2)$$

121 Co-latitude theta is measured from Enceladus's south pole, and $\theta_0 = 30^\circ$ is the plume half-
 122 width, based on INMS in situ observations [*Smith et al.*, 2010]. We assume no azimuthal
 123 dependence.

124 Enceladus's gravity is ignored since the escape velocity, $v_{\text{esc}} = 240 \text{ m s}^{-1}$, is greatly
 125 exceeded for most molecules (99%), where $v_{\text{bulk}} > v_{\text{therm}} > v_{\text{esc}}$; our results differ by less
 126 than one percent whether Enceladus's gravity is considered or not. Particles released from
 127 Enceladus are thus assumed to move on Keplerian orbits with respect to Saturn. Each

128 water molecule is allowed to orbit inside the torus for a period determined by the collective
 129 lifetimes against photodissociation, electron-impact dissociation, and charge exchange. To
 130 be clear, the molecules forming the neutral torus are subject to all of the losses stated,
 131 while the neutral cloud is subject to photo-processes only (section 2.2). Further reaction
 132 details are important for modeling plasma characteristics but only the timescales given
 133 below are required to model the neutral torus.

134 **Photodissociation:** The photodissociation lifetime for H_2O , $\tau_{\text{phot}} = 9.1 \times 10^6$ s, comes
 135 directly from *Huebner and Carpenter [1979]*, scaled to Saturn's distance from the Sun. At
 136 peak solar activity, neutral abundances attributed to dissociation double [*Jackman and*
 137 *Arridge, 2011*].

138 **Impact dissociation:** In the case of impact dissociation, suprathermal (hot) electrons
 139 dominate [*Fleshman et al., 2010b*]. Assuming the conditions near Enceladus's orbit apply
 140 throughout the neutral torus, we estimate the hot electron density and temperature to
 141 be 160 eV and 0.3 cm^{-3} from *Fleshman et al. [2010b]*, which fit within a range of recent
 142 observations (cf., *Young et al. [2005]*, *Sittler et al. [2008]*). The rate coefficient for impact
 143 dissociation of water is found by convolving $\sigma(v)v$ with a 160 eV Maxwellian distribution
 144 to find $\kappa_{\text{imp}} = 1.5 \times 10^{-6} \text{ cm}^3 \text{ s}^{-1}$ (*Fleshman et al. [2010b]*, table S9). Above 100 eV,
 145 κ_{imp} is insensitive to temperature, making this estimate valid for a range of observations.
 146 Assuming the hot electron density, n_{eh} , is constant over the neutral torus, the lifetime
 147 against impact dissociation is $\tau_{\text{imp}} \approx [\kappa_{\text{imp}} n_{\text{eh}}]^{-1} = 2.2 \times 10^6$ s. Dissociation *via* thermal
 148 electrons—whose temperature and density are 2 eV and 60 cm^{-3} —is also expected, but
 149 such collisions occur $5 \times$ less often (*Fleshman et al. [2010b]*, table S9) and are thus ignored
 150 here.

151 **Charge exchange:** The following three reactions are included in this study:



152 Other charge exchanges are important in the neutral torus, some of which involve ions
 153 reacting with secondary neutrals such as H, O, and OH. To model their effect properly,
 154 one would calculate these neutral densities as in a conventional time-dependent neutral
 155 cloud model. We estimate that including all such reactions would increase our estimates
 156 on neutral cloud densities by approximately a factor of two. The primary purpose of
 157 choosing this combination of reactions is to study three classes of charge exchanges, for
 158 which the collision frequency decreases with, increases with, or is independent of the
 159 relative speed of the reacting pair (reactions 3b, 3c, and 3a, respectively). We return to
 160 this point in section 2.2.2.

161 An estimate of the charge exchange lifetime can be made by adding the rate co-
 162 efficients for reactions 3a–3c. Multiplying by the observed H_2O^+ and O^+ densities
 163 near the orbit of Enceladus (6 and 12 cm^{-3} , *Sittler et al.* [2008]), we find $\tau_{\text{chex}} =$
 164 $[\kappa_{\text{exch}}^{\text{H}_2\text{O}^+} n_{\text{H}_2\text{O}^+} + \kappa_{\text{exch}}^{\text{O}^+} n_{\text{O}^+}]^{-1} = [6.0 + 2.8]^{-1} \times 10^8 \text{ s} = 1.1 \times 10^7 \text{ s}$. The reaction rates
 165 are from *Lishawa et al.* [1990] and *Albritton* [1978] for $\kappa_{\text{exch}}^{\text{H}_2\text{O}^+}$ and $\kappa_{\text{exch}}^{\text{O}^+}$, respectively. The
 166 lifetime of H_2O against the sum of these processes is then

$$\begin{aligned} \tau_{\text{torus}} &= \left[\frac{1}{\tau_{\text{phot}}} + \frac{1}{\tau_{\text{imp}}} + \frac{1}{\tau_{\text{chex}}} \right]^{-1} = (1.1 + 4.5 + 0.91)^{-1} \times 10^7 \text{ s} \\ &= 1.6 \times 10^6 \text{ s} \approx 20 \text{ days}. \end{aligned} \quad (4)$$

167 These estimates can be compared to Fig. 3 of *Cassidy and Johnson* [2010]: for example,
 168 our lifetime against dissociation is 1.7×10^6 s, while they use 7×10^6 s near $4 R_S$. The
 169 discrepancy comes mostly from the impact dissociation timescale. Cassidy's dissociation
 170 rate was calculated using *Schippers et al.* [2008], wherein CAPS ELS data were fitted and
 171 extapolated down from $5.5 R_S$, while our own estimate hinges on a hot electron density
 172 derived from our chemistry model [*Fleshman et al.*, 2010b]. For charge exchange, we have
 173 a lifetime of 1.1×10^7 s, and *Cassidy and Johnson* [2010] have a comparable 8×10^6 s.

174 Particles are created and tracked in each of our model runs, and the results are scaled
 175 to the number of water molecules in the real neutral torus. The total number is estimated
 176 from an assumed neutral source rate from Enceladus of $\dot{M} = 200 \text{ kg s}^{-1}$ [*Jurac and*
 177 *Richardson*, 2005; *Hansen et al.*, 2006, 2011] and lifetime, τ_{torus} (Eq. 4):

$$N_{\text{torus}} = \dot{M} \tau_{\text{torus}} / m_{\text{H}_2\text{O}} \approx 1.1 \times 10^{34} \text{ H}_2\text{O molecules.} \quad (5)$$

178 We bin and azimuthally average the results to find a 2-D density function, $n_{\text{torus}}(r, \theta)$
 179 (radius and latitude), through which to introduce ions for charge exchange. This function
 180 also determines from where dissociated neutrals are produced.

181 2.1.2. Plume model

182 Before describing dissociation and charge exchange within the torus, we address a cal-
 183 culation with the purpose of comparing the neutral production near Enceladus with that
 184 from the entire torus. In doing so, we prescribe a plume whose density is consistent with
 185 Eqs. 1 and 2. In this case, the ambient neutral density can be ignored compared to the
 186 neutrals leaving the surface of Enceladus directly.

187 The densities are determined everywhere by imposing integrated flux ($\int n(r, \theta) v(r, \theta) dA$)
 188 and energy ($mv^2/2 - mM_E G/r$) conservation at a given distance r . The picture can be

189 simplified, however, since most neutrals have at least twice Enceladus's escape velocity.
 190 The speeds are thus independent of r in the immediate vicinity of Enceladus. By equating
 191 the integrated flux at the surface of Enceladus to the same integral at another distance
 192 $r > R_E$, we find a familiar $1/r^2$ dependence:

$$n_{\text{plume}}(r, \theta) = n(\theta) \left(\frac{R_E}{r} \right)^2 \exp \left[- \left(\frac{r - R_E}{H_r} \right) \right]. \quad (6)$$

193 The trailing exponential factor is imposed *ad hoc* to keep the total plume content finite,
 194 and reflects Saturn's influence as the molecules leave Enceladus. Consistent with *Saur*
 195 *et al.* [2008], H_r is set at 4 times the Hill radius of 948 km. The angular dependence is
 196 consistent with our velocity distribution in the previous section (Eq. 1),

$$n(\theta) = \begin{cases} \frac{n_0}{2} \left[1 + \cos \left(\frac{\theta}{\theta_0} \pi \right) \right] & \text{if } \theta < \theta_0 = 30^\circ \\ 0 & \text{otherwise,} \end{cases} \quad (7)$$

197 which is normalized such that $n(0) = n_0$, where the plume strength n_0 is found to be
 198 $5.9 \times 10^8 \text{ cm}^{-3}$ by integrating $n(\theta)v_{\text{bulk}}$ over the area spanning the south pole of Enceladus
 199 from $\theta = 0^\circ$ to $\theta = \theta_0 = 30^\circ$, and setting that result equal to the plume production rate
 200 of $\dot{M}/m_{\text{H}_2\text{O}} = (200 \text{ kg s}^{-1})/m_{\text{H}_2\text{O}} = 6.7 \times 10^{27}$ molecules per second.

201 In section 3, we compare the results of charge exchange with the plume (n_{plume}) to that
 202 with the entire torus (n_{torus}).

2.2. Neutral cloud model

203 Production of Saturn's neutral clouds entails following the neutrals produced by disso-
 204 ciation and charge exchange occurring within the neutral torus. The treatment of each of
 205 these processes are described below.

2.2.1. Dissociation

207 The hydroxyl radical, OH, produced largely by dissociated H₂O, has previously been
 208 modeled with a single speed of 1 km s⁻¹ (*i.e.*, *Jurac and Richardson [2005], Cassidy and*
 209 *Johnson [2010]*). Dissociated OH has been measured however with speeds between 1 and
 210 1.6 km s⁻¹ [*Wu and Chen, 1993; Makarov et al., 2004*]. Here we bound this range by
 211 modeling the OH neutral clouds produced from an azimuthally-symmetric source (with
 212 respect to Saturn) with velocities drawn from Maxwellian distributions with tempera-
 213 tures $T = \frac{1}{2}m_{\text{OH}}v_{\text{mp}}^2$, where the most probable speed, v_{mp} , is set to 1 and 1.6 km s⁻¹,
 214 representing the low- and high-speed limits.

215 The initial locations of the ejected OH are determined by the spatial distribution of
 216 neutrals in the Enceladus torus ($n_{\text{torus}}(r, \theta)$, section 2.1.1), and the directions of their
 217 release are chosen randomly and isotropically. The molecules orbit Saturn until they are
 218 photodissociated and removed from the system.

219 By assuming a volume over which dissociations occur, the number of modeled OH
 220 molecules can be scaled to a realistic value. We take the volume to be a torus centered
 221 on Enceladus (3.95 R_S), with a minor radius of 1 R_S:

$$V \approx 2\pi(4 R_S)(2 R_S)^2 = 2 \times 10^{31} \text{ cm}^3. \quad (8)$$

222 For impact dissociation, we then expect a contribution of

$$N_{\text{cloud}}^{\text{imp}} = k_{\text{imp}}\tau_{\text{phot}}^{\text{OH}}V = 2.8 \times 10^{34} \text{ OH molecules}, \quad (9)$$

223 where $k_{\text{imp}} = 7.9 \times 10^{-5} \text{ cm}^{-3} \text{ s}^{-1}$ is the rate (per volume) of impact dissociations occurring
 224 between suprathermal electrons and H₂O molecules in the torus [*Fleshman et al., 2010b*]
 225 and $\tau_{\text{phot}}^{\text{OH}} = 1.8 \times 10^7 \text{ s}$ is the photodissociation lifetime of OH at Saturn [*Huebner and*
 226 *Carpenter, 1979*]. The number of OH molecules produced by photodissociation in the

227 torus is similarly given by

$$N_{\text{cloud}}^{\text{phot}} = k_{\text{phot}} \tau_{\text{phot}}^{\text{OH}} V = 7.6 \times 10^{33} \text{ OH molecules}, \quad (10)$$

228 where $k_{\text{phot}} = 2.1 \times 10^{-5} \text{ cm}^{-3} \text{ s}^{-1}$ is the rate (per volume) of H₂O photodissociations
 229 occurring in the Enceladus torus (*Fleshman et al.* [2010b], Table S9). The total abundance
 230 attributed to dissociation is then given by the sum of Eqs. 9 and 10. *Cassidy and Johnson*
 231 [2010] constrained their study with HST observations [*Melin et al.*, 2009] and found a
 232 similar OH content (see comparison in Fig. 10c, this paper).

233 That neutral production by photo- and impact dissociation are comparable in magni-
 234 tude is itself noteworthy. This condition is not shared by systems with hotter and denser
 235 plasma. For example, electron impact dissociation and ionization dominate over photon-
 236 driven processes in Jupiter's Io torus, where the plasma is warmer where the pick-up
 237 energies are four times higher than at Enceladus [*Delamere et al.*, 2007; *Fleshman et al.*,
 238 2010b]. We also note that unlike with Io, long neutral lifetimes in the Enceladus neu-
 239 tral torus inhibit the response of Saturn's neutral clouds to short-term plume variability,
 240 though variability on the order of months has been studied by *Smith et al.* [2010].

241 2.2.2. Charge exchange

242 We now describe the model for producing and following neutrals from charge exchange.
 243 *Cassidy and Johnson* [2010] and *Jurac and Richardson* [2005] also considered velocity-
 244 dependent charge exchange, but unlike these previous studies, we capture the gyrophase
 245 at which the reactions occur by following ions along their trajectories (section 3.1). We
 246 also prescribe cross sections specific to each reaction, being particularly interested in the
 247 effects of low-velocity charge exchange.

At very high speeds, the cross sections go to zero for all charge exchanges [Johnson, 1990]. At low relative velocities, however (few km s⁻¹), the details of the collision are determined by the nature of the reacting species. If the reactants and products are identical, apart from an electron (*i.e.*, H₂O + H₂O⁺ → H₂O⁺ + H₂O*), the reaction is termed resonant, or symmetric, and the cross sections grow as the inverse of the relative speed. If the reactants differ, as with H₂O + O⁺ → H₂O⁺ + O*, the cross sections are likely to vanish at low speeds [Rapp and Francis, 1962]—the difference being that the energy of the electron configurations is unchanged for symmetric-type charge exchanges [Johnson, 1990]. Neutrals produced from resonant charge exchange therefore tend to have lower velocities than do neutrals produced from non-resonant (asymmetric) charge exchange. This is a key point central to much of our discussion in section 3.

Individual ions are followed as they traverse the neutral torus (section 2.1). This approach allows their gyrophase to be determined the instant that charge exchanges occur (see Fig. 1). The implicit assumption is that the collision is elastic, and that the neutral product has an initial velocity given by the ion velocity just before the exchange takes place.

The ions are introduced into the model from two Maxwellian speed distributions,

$$f_{\perp}(v_{\perp}) = \frac{m_{\text{ion}}}{kT_{\perp}} v_{\perp} \exp \left[-\frac{m_{\text{ion}} v_{\perp}^2}{2kT_{\perp}} \right] \quad (\text{speeds perpendicular to } B) \quad (11)$$

$$f_{\parallel}(v_{\parallel}) = \sqrt{\frac{m_{\text{ion}}}{2\pi kT_{\parallel}}} \exp \left[-\frac{m_{\text{ion}} v_{\parallel}^2}{2kT_{\parallel}} \right] \quad (\text{speeds parallel to } B) \quad (12)$$

with a temperature anisotropy of

$$\frac{kT_{\perp}}{kT_{\parallel}} = \frac{27 \text{ eV}}{5.4 \text{ eV}} = 5 \quad (13)$$

266 for both O^+ and H_2O^+ [Sittler *et al.*, 2008]. The perpendicular temperature is derived
 267 from the pick-up ion velocity at the orbit of Enceladus, determined from CAPS data by
 268 Wilson *et al.* [2009] [$kT_{\perp} = \frac{1}{2}m_{\text{W}^+}(v_{\phi} - v_{\text{Kep}})^2$]. The ions also rotate around a guiding
 269 center (field line) moving at $v_{\phi} = 18 \text{ km s}^{-1}$ in a frame rotating with the neutrals.

270 For the component of our study aimed at estimating local neutral production (section
 271 2.1.2), ions passing near Enceladus are diverted (treating Enceladus as a rigid cylinder)
 272 and are slowed to 10% of the ambient flow speed to account for the effects of mass-loading
 273 (see Fleshman *et al.* [2010a]).

274 Time steps are taken at less than 1% of an ion's gyroperiod:

$$\Delta t = R \times T_{\text{gyro}} = R \times \frac{2\pi m}{qB}, \quad (14)$$

275 where R is a random number between 0 and 0.01, T_{gyro} is the ion's gyroperiod (3.6 s for
 276 H_2O^+), $B = 325 \text{ nT}$, and q and m are the charge and mass, respectively, of the reacting ion.
 277 Such resolution is necessary in order to capture the significance of the energy dependence
 278 at low relative speeds. After each time step, the collision frequency ν is calculated from

$$\nu(r, \theta, v_{\text{rel}}) = n(r, \theta)\sigma(v_{\text{rel}})v_{\text{rel}}, \quad (15)$$

279 where $n(r, \theta)$ is the local H_2O density (section 2.1), v_{rel} is the relative velocity between
 280 the reacting ion and neutral, and $\sigma(v_{\text{rel}})$ is the velocity-dependent cross section. Poisson
 281 statistics are used to test the likelihood of one or more reactions having occurred within
 282 Δt . If $\exp(-\nu\Delta t)$ is less than a second random number between 0 and 1, then a reaction
 283 occurs. The possibility of multiple reactions occurring over Δt is taken into account, but
 284 it is neglectable (appendix A).

285 As with OH produced by dissociation (section 2.2.1), neutrals produced by charge ex-
 286 change are followed under the influence of Saturn's gravity until they are photodissociated
 287 or photoionized. Their initial location and velocity are taken to be that of the reacting
 288 ion, pre-transfer.

289 The model runs are centered on the orbit of Enceladus spanning $10 R_E$ in the direction of
 290 corotation ($R_E = 250 \text{ km} = \text{radius of Enceladus}$) and $\pm 120 R_E$ ($0.5 R_S$) in both the radial
 291 and z directions to adequately sample the H_2O torus (section 2.1.1). Ions are introduced
 292 into the model on the upstream boundary, and their guiding centers flow downstream at
 293 a speed $v_{\text{plasma}} = 18 \text{ km s}^{-1}$ relative to the neutrals. Their starting location in (r, z) is
 294 chosen randomly.

295 **Scaling:** The neutral clouds formed *via* charge exchange are done so in our model by
 296 following a relatively small number of ions, and must thus be scaled to facilitate compar-
 297 ison with observations and other models. The number of neutrals in our modeled clouds
 298 have been scaled by accounting for the following. First, the number of representative ions
 299 used to produce the neutral clouds *via* charge exchange falls short of, and must be scaled
 300 to, the number of ions present in the actual plasma torus, $n_{\text{ion}}V$. The volume of the
 301 plasma torus, V , is given in Eq. 8, and $n = 12$ and 6 cm^{-3} for O^+ and H_2O^+ , respectively
 302 [Sittler *et al.*, 2008]. Second, we have argued that photo-processes are more likely to occur
 303 than either charge exchange or electron-impact processes throughout the neutral clouds
 304 with the exception of very near the neutral torus. In keeping with this assumption, the
 305 plasma torus thus feeds the extended neutral clouds *via* charge exchange for a photodisso-
 306 ciation (photoionization in the case of oxygen) time scale before equilibrium of the neutral
 307 cloud is achieved: $\tau_{\text{phot}} = 14, 0.6, 0.3$ years for O, OH, and H_2O , respectively [Fleshman

308 *et al.*, 2010b]. Our model runs followed 10^5 ions for 100 seconds, and the resulting neutral
 309 clouds were scaled as described.

3. Results

310 In the following sections, we present and discuss the neutral clouds resulting from dis-
 311 sociation and charge exchange in our model.

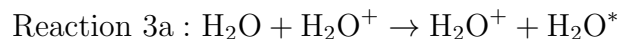
3.1. Charge exchange

312 In the neutrals' reference frame, ions oscillate between ≈ 0 km s $^{-1}$ and twice the local
 313 pick-up speed ($v_\phi \approx 18$ km s $^{-1}$) due to gyro-motion. A cartoon of this can be seen in Fig.
 314 1, where $v_{\text{rel}} \approx 0$ at the cusp of the ion trajectory and reaches a maximum of $v_{\text{rel}} \approx 2v_\phi$
 315 along the flow direction. Shown are several trajectories for which v_\perp is either less than,
 316 greater than, or approximately equal to the bulk flow velocity. The neutrals formed *via*
 317 charge exchange follow the trajectories indicated in red.

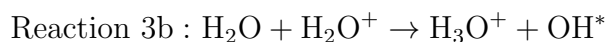
318 The velocity dependence of reactions 3a–3c are determined by the details of the reacting
 319 species [*Johnson*, 1990]. Essentially, symmetric charge exchanges have cross sections that
 320 increase monotonically with decreasing velocity, whereas cross sections for asymmetric
 321 exchange peak and then vanish at low relative speeds. The implication is that symmetric
 322 exchanges produce lower velocity neutrals and a more compact neutral cloud than do
 323 asymmetric reactions.

324 With symmetric charge exchange, the cross sections go as v_{rel}^{-1} , so that the collision
 325 frequency ($n\sigma v$) is independent of v , as with reaction 3a, whereas asymmetric exchanges
 326 are defined by cross sections (and collision frequencies) which tend rapidly toward zero at
 327 low relative velocities ($\sim v_{\text{rel}}^4$, *Rapp and Francis* [1962]).

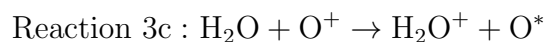
328 The cross sections (10^{-16} cm²) used in this paper to study reactions 3a-3c plotted in
 329 Fig. 2a are given by



$$\sigma_{\text{H}_2\text{O}} = 38E_{\text{rel}}^{-0.5} \quad (16a)$$



$$\sigma_{\text{OH}} = 38E_{\text{rel}}^{-0.88} - 0.39 \exp \left[-\frac{1}{2} \left(\frac{E_{\text{rel}} - 57}{12} \right)^2 \right] \quad (16b)$$



$$\sigma_{\text{O}} = 69E_{\text{rel}}^{-0.29} + 30 \exp \left[-\frac{1}{2} \left(\frac{E_{\text{rel}} - 65}{18} \right)^2 \right]. \quad (16c)$$

330 The Gaussian terms in Eqs. 16b and 16c account for downward and upward trends in the
 331 associated data sets near 30 km s⁻¹, but have little consequence on the neutral cloud,
 332 given that most bound particles are produced at lower velocities.

333 Symmetric exchanges occur between like species by definition, although unlike species
 334 also exhibit symmetric behavior on occasion. Therefore, we explore several hypothetical
 335 behaviors for the OH*-producing reaction 3b at low energies. This test is separate from,
 336 but related to, the comparison between reactions 3a-3c themselves, and it motivates the
 337 point that both high and low energy behaviors have an important effect on the neutral
 338 cloud. With $\sigma_{\text{OH}}^{\text{extrapolated}}$, we have extrapolated the best-fit curve (Eq. 16b) to the lowest
 339 energies. Symmetric and asymmetric behaviors are explored with $\sigma_{\text{OH}}^{\text{symmetric}}$ and $\sigma_{\text{OH}}^{\text{asymmetric}}$
 340 [*Rapp and Francis, 1962; Johnson, 1990*]. $\sigma_{\text{OH}}^{\text{symmetric}}$ is the same as $\sigma_{\text{OH}}^{\text{extrapolated}}$ except that
 341 below 1.5 eV, $\sigma_{\text{OH}}^{\text{symmetric}} = 30E_{\text{rel}}^{-0.5} \times 10^{-16}$ cm². Notice that a similar energy dependence
 342 also applies to Eq. 16a, consistent with symmetric charge exchange. $\sigma_{\text{OH}}^{\text{asymmetric}}$ is the same
 343 as $\sigma_{\text{OH}}^{\text{extrapolated}}$ except that below 1.5 eV, $\sigma_{\text{OH}}^{\text{asymmetric}} = 11E_{\text{rel}}^2 \times 10^{-16}$ cm². Although it could

344 be argued that $\sigma_{\text{OH}}^{\text{symmetric}}$ better fits the data if the two measurements at 2 eV are ignored,
 345 our results for reaction 3b were obtained with $\sigma_{\text{OH}}^{\text{extrapolated}}$ unless noted otherwise. We will
 346 discuss the implications of choosing $\sigma_{\text{OH}}^{\text{extrapolated}}$ over $\sigma_{\text{OH}}^{\text{symmetric}}$ and $\sigma_{\text{OH}}^{\text{asymmetric}}$ shortly.

347 The collision frequencies ($n\sigma v$) are plotted in Fig. 2b for a given neutral density—in
 348 this case for $n_{\text{H}_2\text{O}} = 10^3 \text{ cm}^{-3}$. The collision frequency for oxygen increases with relative
 349 speed, while it is constant for water, and peaks at low velocities for OH. The significance
 350 is that the oxygen cloud tends to be more extended than either the OH or H₂O clouds.
 351 The average collision frequency is also much higher for oxygen ($\times 10$) than for either OH
 352 or H₂O, resulting in greater oxygen abundance.

353 The equatorial neutral cloud densities resulting from reactions 3a–3c are plotted in
 354 Fig. 3. Only neutrals produced from charge exchange are shown; neither the Enceladus
 355 neutral torus, nor the neutrals produced *via* dissociation have been included. Oxygen is
 356 two orders of magnitude more abundant than either OH or H₂O because of the higher rate
 357 of production, but also because oxygen has a longer lifetime against photoionization than
 358 either OH or H₂O have against photodissociation. Unlike *Cassidy and Johnson* [2010],
 359 dissociated neutrals from the latter processes are not tracked in our model. Beyond the
 360 scope of the present study, this additional heating source would serve to further inflate the
 361 oxygen and OH clouds. Fig. 3b is the same as 3a, except that the profiles are normalized
 362 to the peak density at the orbit of Enceladus. The oxygen cloud is seen to be the most
 363 extended, followed by water, and finally by OH, with an order of magnitude separating
 364 the three species at 20 R_S.

365 The effects of low-velocity charge exchange are shown in Fig. 4. In Fig. 4a, we see that
 366 the peak density (as well as the total neutral cloud content) is the highest with $\sigma_{\text{OH}}^{\text{extrapolated}}$

367 because more low-velocity neutrals are produced than with either $\sigma_{\text{OH}}^{\text{symmetric}}$ or $\sigma_{\text{OH}}^{\text{asymmetric}}$.
 368 Conversely, fewer low-velocity neutrals are available to populate the region near Ence-
 369 ladus's orbit with $\sigma_{\text{OH}}^{\text{asymmetric}}$ when compared to either $\sigma_{\text{OH}}^{\text{extrapolated}}$ or $\sigma_{\text{OH}}^{\text{symmetric}}$. Stated
 370 another way, $\sigma_{\text{OH}}^{\text{extrapolated}}$ yields a neutral cloud with the steepest slope, and $\sigma_{\text{OH}}^{\text{asymmetric}}$, the
 371 shallowest. Fig. 4b is identical to Fig. 4a, apart from normalization. In this case, the slope
 372 of the density profile should not be confused with the effect of inflating (spreading) the
 373 OH cloud. It should be viewed, rather, as the enhancement or depletion of low velocity
 374 neutrals to fill the region inside of $\approx 10 R_{\text{S}}$. In other words, neutrals beyond $10 R_{\text{S}}$ are
 375 mostly formed in charge exchanges at high velocities, for which all σ_{OH} converge to the
 376 same curve (Fig. 2).

377 We have assumed to this point that the plasma is sub-corotating in Enceladus's orbit
 378 (18 km s^{-1} , *Wilson et al.* [2009]). One might expect, however, that the neutral cloud
 379 would be affected in a measurable way if instead, the plasma corotates at 26 km s^{-1} .
 380 The H_2O cloud would be least affected, given that the collision frequency of reaction 3a is
 381 independent of speed (Fig. 2b), but what about reactions such as 3b and 3c, whose collision
 382 frequencies are velocity-dependent? Increasing the plasma speed amounts to shifting the
 383 spread of ion velocities in Fig. 2 to the right, which would on average increase the speed
 384 of the neutral products. This is indeed the case, and in such a test where we increased the
 385 plasma speed from 18 to 26 km s^{-1} , the oxygen cloud increased in abundance and became
 386 even more extended. The OH cloud also expanded somewhat, but decreased in total
 387 abundance. Unfortunately, the differences were less than 10% in both the slope of the
 388 distribution and in total oxygen abundance, suggesting that neutral cloud observations
 389 are in this way unlikely to predict plasma speeds in the torus.

3.1.1. Neutral cloud sources: plume *vs.* neutral torus

We described in section 2.1 the production in our model of the neutral H₂O torus from the Enceladus plumes. The plumes themselves have also been prescribed as a separate background density (n_{plume} , section 2.1.2) so that we can compare charge exchange occurring throughout the neutral torus to that occurring only within the Enceladus plumes.

The results are shown in Fig. 5, where we have plotted the oxygen clouds produced from charge exchange within both the Enceladus plumes (local) and the entire neutral torus (global). The results are for reaction 3c, but the same test with reactions 3a and 3b produces similar results. Immediately noticeable is that the local production is $\approx 0.1\%$ of the overall neutral production. The torus's dominance of neutral production can be explained as follows. First, the volume of the torus where reactions are occurring can be estimated as $2\pi(4R_S)(0.2R_S)^2$, where $0.1R_S$ is roughly the torus's scale height. The volume of the plume can be estimated from Eq. 6, where the dimensions are on the order of a cylinder with width $2R_E$ and height $H_r \approx 16R_E$. Dividing these volumes gives roughly $250(R_E/R_S)^3 \approx 10^{-5}$. Further, the collision frequencies are proportional to the neutral density, which in the plume are on the order of 10^7 cm^{-3} , whereas typical torus densities are 10^5 cm^{-3} , making collisions in the plume $100\times$ more frequent per volume than in the torus. All told, the ratio of the volumes (10^{-5}) combined with the ratio of densities (10^2) explain the local-to-global neutral production ratio of 10^{-3} shown in Fig. 5a. A similar pattern has been shown to exist at Jupiter by *Bagenal* [1997] and *Dols et al.* [2008], where the majority of plasma is produced throughout the neutral torus, rather than near the interaction at Io itself.

412 The slopes of the neutral clouds from the plume and torus are most easily compared
 413 in Fig. 5b, in which the density profiles have been normalized. The local source produces
 414 a more confined neutral cloud because the ions from which they originate have been
 415 slowed near the plume to account for the effect of mass-loading (*Fleshman et al.* [2010a]).
 416 Nevertheless, such a signature would be difficult to untangle in the data since global
 417 exceeds local production so overwhelmingly.

3.2. Dissociation

418 A major component of the OH cloud is produced by dissociation within the neutral
 419 torus, whereby the initial velocities of the OH products range from 1 to 1.6 km s⁻¹ [*Wu*
 420 *and Chen*, 1993; *Makarov et al.*, 2004]. In Fig. 6, the clouds resulting from the high- and
 421 low-speed cases are plotted along with the result from velocity-dependent charge exchange
 422 in section 3.1. First note that dissociation contributes 100× more OH than does charge
 423 exchange at the orbit of Enceladus (4 R_S); the total cloud mass is almost 100× greater
 424 as well. Second, dissociation dominates over charge exchange from the Enceladus torus
 425 out to 9 and 15 R_S in the low- and high-speed cases, respectively. The OH cloud content
 426 will only be marginally affected by variable solar activity [*Jackman and Arridge*, 2011],
 427 given that impact dissociation contributes 4× more neutrals than does photodissociation,
 428 by virtue of the respective reaction rates (section 2.2.1). In both cases, few neutrals are
 429 absorbed by the rings, and even less by Saturn itself. The same is not true of charge
 430 exchange, where ≈ 50% of the neutrals are absorbed by Saturn (section 3.3).

431 Fig. 7c is a two-dimensional version of Fig. 6, where the dissociation results have been
 432 averaged and added to the results from charge exchange. Saturn is at the left, and the
 433 Enceladus's orbit is located on the equator at 4 R_S. In addition to being confined radially,

434 the dissociated neutrals are also bound tightly to the equator, while neutrals from charge
 435 exchange tenuously fill the magnetosphere.

436 Fig. 7a shows the hydrogen cloud that accompanies the dissociated OH clouds
 437 ($\text{H}_2\text{O} + e, \gamma \rightarrow \text{OH}^* + \text{H}^*$). To conserve momentum, the hydrogen atoms have $17\times$ the
 438 speed of the dissociated OH molecules, and thus range between 17 and 27 km s^{-1} , with
 439 a relatively large, diffuse neutral cloud. Shown is the result for the low-speed case, which
 440 produces more bound particles and thus a more substantial neutral cloud. Charge ex-
 441 change from reactions such as $\text{H}_2\text{O} + \text{H}^+ \rightarrow \text{H}_2\text{O}^+ + \text{H}^*$ are also responsible for H-cloud
 442 production, and deserve attention in future studies.

3.3. Fates of neutral atoms and molecules

443 In our model, neutrals created by dissociation and charge exchange are eventually either
 444 absorbed by Saturn, escape the system, or orbit until they are destroyed (ionized) by
 445 photons. In Fig. 8a the fates for each species are given by percentage. In the case of
 446 hydrogen, the results are from the dissociation model, described in section 3.2. The
 447 enormous amount of escape (84%) is due to the high velocities ($\approx 17 \text{ km s}^{-1}$) with which
 448 hydrogen is created following H_2O dissociation, and the 8% absorption is largely comprised
 449 of hydrogen which would escape the system otherwise.

450 Oxygen is produced purely from charge exchange in our model (reaction 3c). About one-
 451 half escapes, one-third is absorbed, and the remaining 13% contributes to the neutral cloud
 452 before being photoionized. Water is also produced purely by charge exchange (reaction
 453 3a) with 18% contributing to the neutral cloud. Percentage-wise, more water is absorbed
 454 than oxygen because oxygen is produced with higher speeds and generally larger orbits
 455 (section 3.1).

456 The fate of OH is dominated by dissociation: 96% feed the neutral cloud (ultimately
 457 ionized), 4% are absorbed, and virtually none escape. The reason for the large percentage
 458 of bound and unabsorbed neutrals is that dissociated OH has a velocity spread of 1 to
 459 1.6 km s^{-1} in the neutral frame, compared to the escape speed of $\approx 5 \text{ km s}^{-1}$ in the same
 460 frame. Looking only at OH produced by charge exchange (minor compared to dissocia-
 461 tion), 58% are absorbed, 23% supply the neutral cloud, and 20% escape. Compared to
 462 H_2O , an even greater percentage of charge-exchanged OH is absorbed because the cross
 463 sections favor production of low-velocity OH molecules (Fig. 2b).

464 The production of oxygen *via* dissociation of H_2O has been ignored in this paper on
 465 the grounds that, unlike OH, oxygen is largely produced by charge exchange. The cross
 466 section for oxygen-producing charge exchange is an order of magnitude higher than that
 467 for the OH-producing reaction near the plasma flow speed of $v_{\text{plasma}} = 18 \text{ km s}^{-1}$ (Fig.
 468 2a), while the photodissociation rates are an order of magnitude smaller [*Huebner and*
 469 *Carpenter, 1979*]. We estimate that including oxygen produced from dissociation would
 470 increase the total oxygen cloud content by less than 20%.

471 Charge exchange and dissociation play a large role in creating Saturn's neutral clouds
 472 from the plume-fed neutral torus. The reactions we have included have been chosen to
 473 demonstrate the effects of low velocity charge exchange and dissociation, but they are
 474 also among the most important. The neutral cloud densities presented in this paper are
 475 expected to undershoot the results from models which include the additional reactions
 476 found in Fig. 3, of *Fleshman et al. [2010b]* by no more than a factor of two. With this
 477 caveat in mind, we now compare the present results with several other recent models.

478 3.3.1. Comparison with other models

479 Fig. 8b: J06 is the work of *Johnson et al.* [2006], where they also investigated the neutral
 480 clouds created from low-velocity charge exchange in the stagnated flows in Enceladus's
 481 orbit. Fig. 8b: J07 is from *Jurac and Richardson* [2007], where the authors were primarily
 482 interested in the interaction between the neutral cloud and Saturn's rings. The most
 483 recent model comes from *Cassidy and Johnson* [2010] (C10), where they investigated the
 484 spreading of the neutral cloud from neutral-neutral collisions.

485 To compare with these studies, we first had to weight our H, O, OH, and H₂O clouds.
 486 We did this for two limiting cases. In the first case (τ_{phot} , Fig. 8b), we assume, as we
 487 have thus far, that the neutral clouds evolve until destroyed by either photoionization or
 488 photodissociation: H, O, OH, H₂O = 40, 14, 0.6, 0.3 years, respectively. These lifetimes
 489 yield an upper limit since charge exchange and electron impact are not included as losses.
 490 In the second case (τ_{all}), we derived a lower limit to the lifetimes from Table 2 of *Fleshman*
 491 *et al.* [2010b] by summing the additional losses due to charge exchange and electron
 492 impact, finding: H, O, OH, H₂O = 0.4, 0.4, 0.2, 0.03 years, respectively. Notice in
 493 particular the drastically different times scales for H and O, where including the additional
 494 sinks reduce the size of the H cloud by a factor of $40/0.4 = 100$, and the oxygen cloud
 495 by $14/0.4 = 35$. This case represents an extreme limit, given that the neutrals spend
 496 almost all of their time orbiting outside of the Enceladus torus, where compared to photo-
 497 processes, the chances of charge exchange and electron impact are relatively unlikely. We
 498 mention, however, that *Rymer et al.* [2007, 2008] has shown that circulation patterns
 499 inside of $12 R_S$ at Saturn gives rise to 'butterfly' hot electron pitch angle distributions,
 500 related to low temperature anisotropy (T_{\perp}/T_{\parallel}), on which proton field-aligned distributions
 501 depend [*Sittler et al.*, 2008].

502 The individual clouds (excluding hydrogen) were weighted by the stated time scales
503 and totaled in Fig. 8b. When only losses to photodissociation/ionization are considered
504 (τ_{phot}), the neutral cloud is dominated by oxygen, whose fate thus determines that of
505 the neutral cloud. When charge exchange and electron impact are also included (τ_{all}),
506 dissociated OH contributes significantly, driving the neutral cloud (ionized) percentage
507 up, and the escape percentage down. We note that the neutral fates presented in *Bagenal*
508 *and Delamere* [2011] (escape = 44%, ionized = 17%, absorbed = 39%) were based on an
509 earlier version of our model which only included H₂O.

510 The particles that are neither absorbed nor lost by escape make up the neutral clouds.
511 In the case where the cloud evolves for τ_{phot} , oxygen and hydrogen dominate since they
512 are far less likely to be photoionized than are OH and H₂O to be photodissociated. With
513 charge exchange and electron impact included (τ_{all}), however, more oxygen and hydrogen
514 are removed from the system, which then tends to favor a molecular OH–H₂O cloud. In
515 terms of total mass the same applies, although hydrogen accounts for only a few percent
516 at most. We find that the total cloud mass is bounded between ≈ 1 and 10 Mtons, for
517 τ_{all} and τ_{phot} , respectively.

518 It is worth pausing to re-emphasize that the system is in reality better represented by the
519 τ_{phot} case, from which all neutral clouds in this paper have been derived. The τ_{all} case is
520 strictly valid only for neutrals within the Enceladus torus, though reactions with electrons
521 and protons may also prove important, as discussed above. What is illustrated, however,
522 is that Saturn's magnetosphere is less oxygen-dominated than suggested by looking at
523 losses from photo-processes alone. These results suggest that our oxygen abundances are
524 somewhat overestimated, likely by less than a factor of two.

525 3.3.2. Neutral absorption

526 The particles absorbed by Saturn and its rings are plotted by species and latitude in
 527 Fig. 9. In Fig. 9b, we see that most absorption comes from oxygen (74%), followed by H₂O
 528 (11%), OH (9%), and finally by hydrogen (6%). Absorption is equally divided between
 529 Saturn and its rings except in the case of OH, where twice as much falls on Saturn's
 530 rings. This is because OH is largely produced by impact dissociation, which creates
 531 slower neutrals than does charge exchange, whereby in our model, H₂O and oxygen arise
 532 exclusively.

533 In Fig. 9b, absorption is plotted against Saturn's latitude. Because the model is sym-
 534 metric about the equator, the results apply to either hemisphere. Oxygen, water, and OH
 535 follow the same trends because they all originate from charge exchange (dissociated OH is
 536 slow and does not reach Saturn), and have been created from ions with similar velocity dis-
 537 tributions. Any second-order differences due to the velocity-dependence of the respective
 538 cross sections are not immediately apparent. Hydrogen, on the other hand, is produced
 539 entirely by dissociation in the model and exhibits a more uniform flux across Saturn. The
 540 explanation is that the velocity distribution from which hydrogen is produced is isotropic,
 541 whereas that which produces charge-exchanged neutrals is bi-Maxwellian (section 2.2.2).
 542 The fluxes shown in Fig. 9b are consistent with *Hartogh et al.* [2011], who modeled recent
 543 Herschel observations of Saturn's water torus and found an average flux of $6 \times 10^5 \text{ cm}^{-2}$
 544 s^{-1} for H₂O + OH impinging on Saturn.

4. Discussion

545 Some useful conclusions can be drawn by further contrasting our results with *Cassidy*
 546 *and Johnson* [2010] (C10). It is important that we first mention a profound difference

547 between our models. The model of C10 effectively carries out resonant charge exchange
 548 only, which does not chemically alter the neutral population; neutrals in their model are
 549 produced either directly from Enceladus or from subsequent dissociations. Neutrals in
 550 our model, on the other hand, originate from Enceladus (H_2O). OH is then created *via*
 551 dissociation (as with C10), but secondary O, OH, and H_2O populations are *created* from
 552 H_2O *via* charge exchange with the dense plume-fed Enceladus torus. The C10 model re-
 553 distributes neutrals around Saturn, while we redistribute and chemically re-assign neutral
 554 abundances by allowing for asymmetric charge exchanges. Thus, it may well be a coinci-
 555 dence that our models are similar in total abundance. While it may be difficult to compare
 556 our total abundances, the slope of our radial density profiles can be contrasted directly
 557 because our redistribution mechanisms (charge exchange and dissociation) are similar.
 558 Differences are due largely to C10's inclusion of neutral collisions and our prescribing
 559 unique velocity-dependent charge exchange for each of the O-, OH-, and H_2O -producing
 560 reactions (reactions 3a–3c).

561 Our neutral clouds are compared with C10 in Fig. 10. All of our clouds include contri-
 562 butions from charge exchange, but the H_2O cloud is mostly comprised of water sourced
 563 directly from Enceladus ($3.95 R_S$), and OH includes the additional source from dissocia-
 564 tion. In the C10 model, the water molecules were spread due to neutral–neutral collisions,
 565 which explains our higher H_2O densities near Enceladus's orbit (Fig. 10a). The slope of
 566 the oxygen profile agrees best with C10 because their charge exchange cross section most
 567 resembles our own (Eq. 16c). Our H_2O profiles agree less, and our OH slopes, the least,
 568 due mainly to the strong effect that neutral collisions have on those more polar molecules.
 569 In particular, C10 used a much larger cross section for neutral collisions involving H_2O

570 and OH [*Teske et al.*, 2005] than for atomic oxygen [*Bondi*, 1964]. This helps to further
571 explain our agreement with their oxygen profile since we exclude neutral–neutral collisions
572 from our model altogether. We conclude that neutral–neutral collisions appear to play a
573 less significant role with atomic species, such as oxygen and hydrogen.

574 The column densities (Fig. 10b) are similar to C10, who constrained their O and OH
575 clouds with the most recent Cassini UVIS results of *Melin et al.* [2009]. Our oxygen
576 density—as well as our total oxygen content (Fig. 10c)—is higher for two reasons. First, we
577 use a larger cross section than does C10 for reaction 3c, and second, the clouds presented
578 here have been limited only by photoionization. Charge exchange and electron impact are
579 second order losses beyond 6 R_S , but including them would favorably reduce the oxygen
580 content more than OH and H_2O (section 3.3), bringing our models into better agreement.

581 Our total H_2O content is $4\times$ less than C10 found (Fig. 10c). This is partly because we
582 have subjected H_2O molecules in the primary (plume-fed) neutral torus to the shortest
583 lifetimes possible (section 2.1.1), whereas C10 tracks molecules that get kicked out of
584 the densest plasma *via* neutral collisions, and thus survive longer, being less susceptible
585 to both charge exchange and electron impact. That their total H_2O content is higher
586 than ours (Fig. 10c), does not contradict the fact that their H_2O column density is lower;
587 neutral–neutral collisions would spread out the torus, lowering the column density, while
588 allowing neutrals to survive longer, increasing the total abundance.

589 Our model would benefit by including the redistribution attributed to neutral collisions
590 by allowing particles to interact in a direct simulation Monte Carlo (DSMC) model such
591 as in C10. Likewise, DSMC models would benefit by including charge exchange cross

592 sections specific to each reaction. Such models should also take into account asymmetric
 593 charge exchanges, which affects neutral cloud composition.

594 The reactions modeled in this study were chosen in order to measure the effect of
 595 symmetric and asymmetric charge exchange at low velocities. Building upon our find-
 596 ings, future studies should include additional neutral-producing charge exchanges, such as
 597 $\text{OH}^+ + \text{H}_2\text{O} \rightarrow \text{OH}^* + \text{H}_2\text{O}^+$, $\text{H}^+ + \text{H}_2\text{O} \rightarrow \text{H}^* + \text{H}_2\text{O}^+$, and $\text{OH}^+ + \text{H}_2\text{O} \rightarrow \text{O}^* + \text{H}_3\text{O}^+$,
 598 as well as dissociative recombination of H_2O^+ .

5. Conclusions

599 We have modeled low-velocity charge exchange from the point of view of the ions,
 600 allowing us to study the effects of velocity as well as gyrophase. With reactions 3a–3c,
 601 we have been able to offer an estimate on the size and shape of the neutral clouds at
 602 Saturn, while simultaneously exploring the sensitivity of the neutral clouds to a variety
 603 of velocity-dependent reactions.

604 We have also re-visited the production of OH following H_2O dissociation in the primary
 605 neutral torus. Previous models have used 1 km s^{-1} as the initial velocity for OH, while
 606 measurements suggest a range of speeds from 1 to 1.6 km s^{-1} . In our model, the higher
 607 speed increases the range within which dissociation dominates neutral production from 9
 608 to $15 R_S$.

609 Additional findings are:

610 (1.) Charge exchange cross sections that increase steeply at low speeds tend to produce
 611 neutral clouds more confined to the orbit of Enceladus, implying the most spreading for
 612 oxygen, moderate spreading for H_2O , and the least for OH (Fig. 3). Accounting for

613 gyrophase doubles the local OH density within Enceladus's orbit, has \approx no effect on H₂O,
 614 and decreases oxygen density by less than 10%.

615 (2.) Enceladus is solely responsible for the creation of the neutral H₂O torus *via* thermal
 616 ejection from its plumes. However, Saturn's neutral clouds are overwhelmingly produced
 617 by charge exchange and dissociation occurring throughout the torus (99%), and not near
 618 Enceladus itself (Fig. 5).

619 (3.) We estimate that roughly half of all neutrals escape the system, with the remaining
 620 equally divided between absorption by the rings/planet and the neutral clouds (Fig. 8).
 621 Less than 50 kg s⁻¹ is thus ionized and transported out of the system as plasma. This
 622 number is expected to represent an upper limit, given we have assumed that all particles
 623 forming the neutral clouds are ultimately ionized; a more accurate result would require
 624 modeling the detailed effects of charge exchange and neutral-neutral collisions within the
 625 neutral clouds. This estimate can be compared to *Sittler et al.* [2008], whose Figs. 14 and
 626 17 give roughly $([NL^2]_{W^+}/L^2) \times m_{W^+}/\tau_{\text{transport}} \approx 3 \times 10^{31} \times m_{W^+}/10^5 \text{ s} \approx 10 \text{ kg s}^{-1}$ at
 627 $L = 10$.

628 (4.) Saturn's neutral cloud has a total mass of at least 1 Mton, but likely much closer
 629 to 10 Mtons. The primary plume-fed neutral torus (0.3 Mtons) is comprised entirely of
 630 water in our model, while the secondary neutral clouds are broken down into H ($\lesssim 5\%$),
 631 O ($\lesssim 82\%$), OH ($\gtrsim 13\%$), and H₂O ($\approx 1\%$). Atomic oxygen dominates the composition
 632 both because of a high production rate from charge exchange as well as a long lifetime
 633 against photoionization. Charge exchange and reactions with electrons favorably remove
 634 hydrogen and oxygen, but are secondary loss mechanisms throughout the majority of the
 635 magnetosphere.

636 (5.) Our model predicts fluxes on Saturn from charge exchange of $\approx 6 \times 10^5 \text{ cm}^{-2} \text{ s}^{-1}$
637 for both OH and H₂O (consistent with Herschel observations by *Hartogh et al.* [2011]),
638 and oxygen is about 5× higher. Absorption is divided equally between Saturn and its
639 rings (Fig. 9a).

640 (6.) Our total neutral abundances are similar to *Cassidy and Johnson* [2010] (C10) for
641 both OH and H₂O, and 4× higher for oxygen (Fig. 10). Differences in the slopes of our
642 equatorial density profiles are in part due to our not including neutral–neutral collisions,
643 while this fact appears to have no effect on the oxygen profile. On the other hand, C10
644 did not include the effects on neutral chemistry following asymmetric charge exchanges,
645 nor did they use velocity-dependent cross sections particular to each reaction. Herschel
646 observations by *Hartogh et al.* [2011] confirm the importance of neutral–neutral collisions
647 for H₂O, but if oxygen is the dominant neutral species in Saturn’s magnetosphere, as
648 our model predicts, neutral–neutral collisions may play a smaller role in Saturn’s neutral
649 cloud than previously expected.

650 Given the effect on both the size and shape of the neutral clouds, we suggest that
651 future neutral cloud models include charge exchange cross sections unique to each reaction.
652 Asymmetric charge exchange also has an important effect on neutral chemistry that should
653 be implemented. Regarding the ions’ gyrophase, Monte Carlo models can account for
654 its effect by using phase-dependent probability distributions. Finally, the range of OH
655 velocities studied here should be considered when modeling dissociation.

656 Moving forward, we plan to implement these suggestions into the neutral cloud model
657 of C10 and to couple that model with the chemistry model of *Fleshman et al.* [2010b].
658 Constrained by Cassini plasma observations, the chemistry model uses C10’s neutrals as

659 input, and provides ion temperatures and densities throughout the magnetosphere (< 20
 660 R_S), which C10 in turn uses to update neutral densities. An improved understanding of
 661 two issues is planned: (1) Where does plasma transport become important? (2) What is
 662 the role of hot electrons with regard to ion-neutral chemistry inside $20 R_S$?

Appendix A: Collision probability

663 The average number of collisions occurring during a time interval Δt is given by $\lambda \equiv$
 664 $\nu \Delta t$, where $\nu = n_{\text{neutrals}} \sigma(v_{\text{rel}}) v_{\text{rel}}$ is the local collision frequency, assumed to be constant
 665 during Δt . Statistics are applied to determine if and how many reactions occur during Δt .
 666 The Poisson distribution [Zwillinger and Company, 1996; Reif, 1965] gives the probability
 667 of suffering exactly n collisions for a given λ :

$$f(n; \lambda) = \frac{e^{-\lambda} \lambda^n}{n!}. \quad (\text{A1})$$

668 Notice that Eq. A1 peaks at $n = \lambda$ if one treats n as a continuous variable. Summing Eq.
 669 A1 discretely from $n = k$ to $n = \infty$ gives the probability of suffering *at least* k collisions
 670 during Δt ,

$$P_k(\lambda) = e^{-\lambda} \sum_{n=k}^{\infty} \frac{\lambda^n}{n!}. \quad (\text{A2})$$

671 Because Eq. A1 is normalized ($e^{-\lambda} \sum_{n=0}^{\infty} \lambda^n/n! = e^{-\lambda} e^{\lambda} = 1$), Eq. A2 can be conveniently
 672 rewritten as

$$P_k(\lambda) = 1 - e^{-\lambda} \sum_{n=0}^{k-1} \frac{\lambda^n}{n!}. \quad (\text{A3})$$

673 A random number ($0 < N < 1$) is compared to each P_k at each timestep. The largest k
 674 for which $P_k > N$ determines how many fast neutrals (collisions), k , are produced during
 675 Δt .

676 In practice, it is only necessary to compare to the first few P_k when $\lambda \ll 1$, made evident
 677 by the leading terms in Eq. A2 for $k + 1$ and k :

$$\frac{P_{k+1}}{P_k} \approx \frac{f(k+1; \lambda)}{f(k; \lambda)} = \frac{\lambda^{k+1}/(k+1)!}{\lambda^k/k!} = \frac{\lambda}{k+1} \xrightarrow{\lambda \rightarrow 0} 0. \quad (\text{A4})$$

678 Multiple collisions are thus increasingly unlikely when $\lambda \ll 1$. In such cases, comparison
 679 with $P_1 = 1 - e^{-\lambda} \approx \lambda = \nu \Delta t$ is sufficient.

680 **Acknowledgments.** This work was supported under the NESSF program, fellowship
 681 number 11-Planet11R-0005. BF thanks two reviewers for their feedback and many useful
 682 suggestions.

References

- 683 Albritton, D. L. (1978), Ion-neutral reaction-rate constants measured in flow reactors
 684 through 1977, *Atomic Data and Nuclear Data Tables*, *22*(1), 1 – 89, doi:10.1016/0092-
 685 640X(78)90027-X.
- 686 Bagenal, F. (1997), Ionization source near Io from Galileo wake data, *Geophys. Res. Lett.*,
 687 *24*, 2111, doi:10.1029/97GL02052.
- 688 Bagenal, F., and P. A. Delamere (2011), Flow of mass and energy in the magnetospheres
 689 of Jupiter and Saturn, *Journal of Geophysical Research (Space Physics)*, *116*, A05,209,
 690 doi:10.1029/2010JA016294.
- 691 Bondi, A. (1964), van der waals volumes and radii, *Journal of Physical Chemistry*, *68*(3),
 692 441–451.
- 693 Cassidy, T. A., and R. E. Johnson (2010), Collisional spreading of Enceladus's neutral
 694 cloud, *Icarus*, *209*, 696–703, doi:10.1016/j.icarus.2010.04.010.

- 695 Delamere, P. A., F. Bagenal, V. Dols, and L. C. Ray (2007), Saturn's neutral torus versus
696 Jupiter's plasma torus, *Geophys. Res. Lett.*, , *34*, L09,105, doi:10.1029/2007GL029437.
- 697 Dols, V., P. A. Delamere, and F. Bagenal (2008), A multispecies chemistry model of
698 Io's local interaction with the Plasma Torus, *Journal of Geophysical Research (Space*
699 *Physics)*, *113*, 9208–+, doi:10.1029/2007JA012805.
- 700 Esposito, L. W., et al. (2005), Ultraviolet Imaging Spectroscopy Shows an Active Satur-
701 nian System, *Science*, *307*, 1251–1255, doi:10.1126/science.1105606.
- 702 Farmer, A. J. (2009), Saturn in hot water: Viscous evolution of the Enceladus torus,
703 *Icarus*, *202*, 280–286, doi:10.1016/j.icarus.2009.02.031.
- 704 Fleshman, B. L., P. A. Delamere, and F. Bagenal (2010a), Modeling the Enceladus plume-
705 plasma interaction, *Geophys. Res. Lett.*, , *37*, L03,202, doi:10.1029/2009GL041613.
- 706 Fleshman, B. L., P. A. Delamere, and F. Bagenal (2010b), A sensitivity study of
707 the Enceladus torus, *Journal of Geophysical Research (Planets)*, *115*, 4007–+, doi:
708 10.1029/2009JE003372.
- 709 Hansen, C. J., L. Esposito, A. I. F. Stewart, J. Colwell, A. Hendrix, W. Pryor, D. She-
710 mansky, and R. West (2006), Enceladus' Water Vapor Plume, *Science*, *311*, 1422–1425,
711 doi:10.1126/science.1121254.
- 712 Hansen, C. J., et al. (2011), The composition and structure of the Enceladus plume,
713 *Geophys. Res. Lett.*, , *381*, L11,202, doi:10.1029/2011GL047415.
- 714 Hartogh, P., et al. (2011), Direct detection of the Enceladus water torus with Herschel,
715 *Astron. Astrophys.*, , *532*, L2+, doi:10.1051/0004-6361/201117377.
- 716 Huebner, W. F., and C. W. Carpenter (1979), Solar photo rate coefficients, *NASA*
717 *STI/Recon Technical Report N, 80*, 24,243–+.

- 718 Jackman, C. M., and C. S. Arridge (2011), Solar Cycle Effects on the Dynamics of Jupiter's
719 and Saturn's Magnetospheres, *Solar Physics*, pp. 77–+, doi:10.1007/s11207-011-9748-
720 Z.
- 721 Johnson, R. E. (1990), *Energetic Charged-Particle Interactions with Atmospheres and*
722 *Surfaces*.
- 723 Johnson, R. E., H. T. Smith, O. J. Tucker, M. Liu, M. H. Burger, E. C. Sittler, and R. L.
724 Tokar (2006), The Enceladus and OH Tori at Saturn, *Astrophys. J.*, , 644, L137–L139,
725 doi:10.1086/505750.
- 726 Jurac, S., and J. D. Richardson (2005), A self-consistent model of plasma and neutrals at
727 Saturn: Neutral cloud morphology, *Journal of Geophysical Research (Space Physics)*,
728 110, 9220–+, doi:10.1029/2004JA010635.
- 729 Jurac, S., and J. D. Richardson (2007), Neutral cloud interaction with Saturn's main
730 rings, *Geophys. Res. Lett.*, , 34, L08,102, doi:10.1029/2007GL029567.
- 731 Jurac, S., M. A. McGrath, R. E. Johnson, J. D. Richardson, V. M. Vasyliunas, and
732 A. Eviatar (2002), Saturn: Search for a missing water source, *Geophys. Res. Lett.*, ,
733 29(24), 2172, doi:10.1029/2002GL015855.
- 734 Li, X., Y.-L. Huang, G. D. Flesch, and C. Y. Ng (1995), Absolute total cross sections for
735 the ion-molecule reaction $O^+(^4S^o)+H_2O$, *Journal of Chemical Physics*, 102, 5100–5101,
736 doi:10.1063/1.469561.
- 737 Lishawa, C. R., R. A. Dressler, J. A. Gardner, R. H. Salter, and E. Murad (1990), Cross
738 sections and product kinetic energy analysis of $h_2o+?h_2o$ collisions at suprathemal
739 energies, 93(5), 3196–3206, doi:DOI:10.1063/1.458852.

- 740 Makarov, O. P., J. M. Ajello, P. Vattipalle, I. Kanik, M. C. Festou, and A. Bhardwaj
741 (2004), Kinetic energy distributions and line profile measurements of dissociation prod-
742 ucts of water upon electron impact, *Journal of Geophysical Research (Space Physics)*,
743 *109*, A09,303, doi:10.1029/2002JA009353.
- 744 Melin, H., D. E. Shemansky, and X. Liu (2009), The distribution of atomic hydrogen
745 and oxygen in the magnetosphere of Saturn, *Planetary Space Science*, *57*, 1743–1753,
746 doi:10.1016/j.pss.2009.04.014.
- 747 Porco, C. C., et al. (2006), Cassini Observes the Active South Pole of Enceladus, *Science*,
748 *311*, 1393–1401, doi:10.1126/science.1123013.
- 749 Rapp, D., and W. E. Francis (1962), Charge Exchange between Gaseous Ions and Atoms,
750 *Journal of Chemical Physics*, *37*, 2631–2645, doi:10.1063/1.1733066.
- 751 Reif, F. (1965), *Fundamentals of statistical and thermal physics / [by] F. Reif*, interna-
752 tional student ed. ed., x, 651 p. : pp., McGraw-Hill Kogakusha, Tokyo :.
- 753 Rymer, A. M., B. H. Mauk, T. W. Hill, C. Paranicas, D. G. Mitchell, A. J. Coates,
754 and D. T. Young (2008), Electron circulation in Saturn's magnetosphere, *Journal of*
755 *Geophysical Research (Space Physics)*, *113*, A01201, doi:10.1029/2007JA012589.
- 756 Rymer, A. M., et al. (2007), Electron sources in Saturn's magnetosphere, *Journal of*
757 *Geophysical Research (Space Physics)*, *112*, A02201, doi:10.1029/2006JA012017.
- 758 Saur, J., N. Schilling, F. M. Neubauer, D. F. Strobel, S. Simon, M. K. Dougherty, C. T.
759 Russell, and R. T. Pappalardo (2008), Evidence for temporal variability of Enceladus'
760 gas jets: Modeling of Cassini observations, *Geophys. Res. Lett.*, , *35*, L20,105, doi:
761 10.1029/2008GL035811.

- 762 Schippers, P., et al. (2008), Multi-instrument analysis of electron populations in Saturn's
763 magnetosphere, *Journal of Geophysical Research (Space Physics)*, *113*, 7208–+, doi:
764 10.1029/2008JA013098.
- 765 Shemansky, D. E., and D. T. Hall (1992), The distribution of atomic hydrogen in the
766 magnetosphere of Saturn, *J. Geophys. Res.*, , *97*, 4143–4161, doi:10.1029/91JA02805.
- 767 Shemansky, D. E., P. Matheson, D. T. Hall, H. Hu, and T. M. Tripp (1993), Detec-
768 tion of the hydroxyl radical in the Saturn magnetosphere, *Nature*, *363*, 329–331, doi:
769 10.1038/363329a0.
- 770 Sittler, E. C., et al. (2005), Preliminary results on Saturn's inner plasmasphere as ob-
771 served by Cassini: Comparison with Voyager, *Geophys. Res. Lett.*, , *32*, 14–+, doi:
772 10.1029/2005GL022653.
- 773 Sittler, E. C., et al. (2008), Ion and neutral sources and sinks within Saturn's
774 inner magnetosphere: Cassini results, *Planetary Space Science*, *56*, 3–18, doi:
775 10.1016/j.pss.2007.06.006.
- 776 Smith, H. T. (2006), The search for nitrogen in Saturn's magnetosphere, Ph.D. thesis,
777 University of Virginia, Virginia, USA.
- 778 Smith, H. T., R. E. Johnson, and V. I. Shematovich (2004), Titan's atomic and molecular
779 nitrogen tori, *Geophys. Res. Lett.*, , *311*, L16,804, doi:10.1029/2004GL020580.
- 780 Smith, H. T., R. E. Johnson, M. E. Perry, D. G. Mitchell, R. L. McNutt, and D. T.
781 Young (2010), Enceladus plume variability and the neutral gas densities in Saturn's
782 magnetosphere, *Journal of Geophysical Research (Space Physics)*, *115*, 10,252–+, doi:
783 10.1029/2009JA015184.

- 784 Smith, H. T., et al. (2007), Enceladus: The likely dominant nitrogen source in Saturn's
785 magnetosphere, *Icarus*, *188*, 356–366, doi:10.1016/j.icarus.2006.12.007.
- 786 Spencer, J. R., et al. (2006), Cassini Encounters Enceladus: Background and the Discovery
787 of a South Polar Hot Spot, *Science*, *311*, 1401–1405, doi:10.1126/science.1121661.
- 788 Teske, V., E. Vogel, and E. Bich (2005), Viscosity measurements on water vapor and
789 their evaluation, *Journal of Chemical & Engineering Data*, *50*(6), 2082–2087, doi:
790 10.1021/je050288d.
- 791 Weiser, H., R. C. Vitz, and H. W. Moos (1977), Detection of Lyman-alpha emis-
792 sion from the Saturnian disk and from the ring system, *Science*, *197*, 755–757, doi:
793 10.1126/science.197.4305.755.
- 794 Wilson, R. J., R. L. Tokar, and M. G. Henderson (2009), Thermal ion flow in Saturn's
795 inner magnetosphere measured by the Cassini plasma spectrometer: A signature of the
796 Enceladus torus?, *Geophys. Res. Lett.*, , *36*, 23,104–+, doi:10.1029/2009GL040225.
- 797 Wu, C. Y. R., and F. Z. Chen (1993), Velocity distributions of hydrogen atoms and
798 hydroxyl radicals produced through solar photodissociation of water, *J. Geophys. Res.*,
799 , *98*, 7415–7435, doi:10.1029/92JE03016.
- 800 Young, D. T., et al. (2005), Composition and Dynamics of Plasma in Saturn's Magneto-
801 sphere, *Science*, *307*, 1262–1266, doi:10.1126/science.1106151.
- 802 Zwillinger, D., and C. R. Company (1996), *CRC standard mathematical tables and for-*
803 *mulae*, no. v. 30 in CRC Standard Mathematical Tables & Formulae, CRC Press.

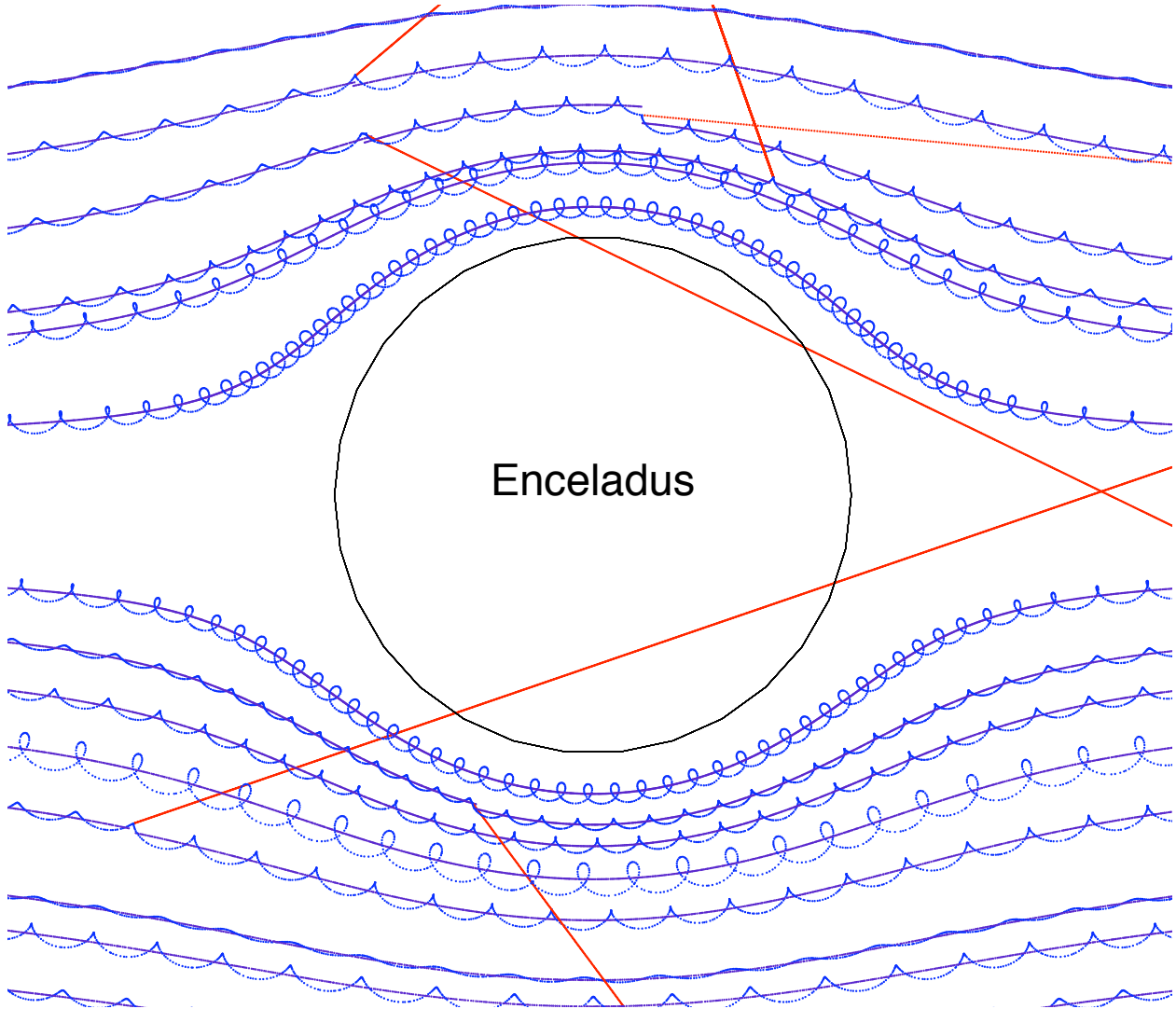


Figure 1. Sketch of gyrating ions in the neutral frame with guiding centers moving along a prescribed flow field, shown here near Enceladus for scale. Warm ions ($v_{\perp} > v_{\text{flow}}$) move on trajectories that coil around themselves and do not reach zero relative velocity with respect to the neutrals at any point. Cool ions ($v_{\perp} < v_{\text{flow}}$) essentially trace their guiding centers with ‘snake-like’ trajectories, and also do not obtain zero relative velocity. Fresh pick-up ions ($v_{\perp} \approx v_{\text{flow}}$) do, however, obtain zero relative velocity at the cusps of their cycloidal trajectories. Neutrals produced by charge exchange (whose trajectories are indicated by the red lines) tend to be created with velocities at which the respective reaction rates peak (Fig. 2).

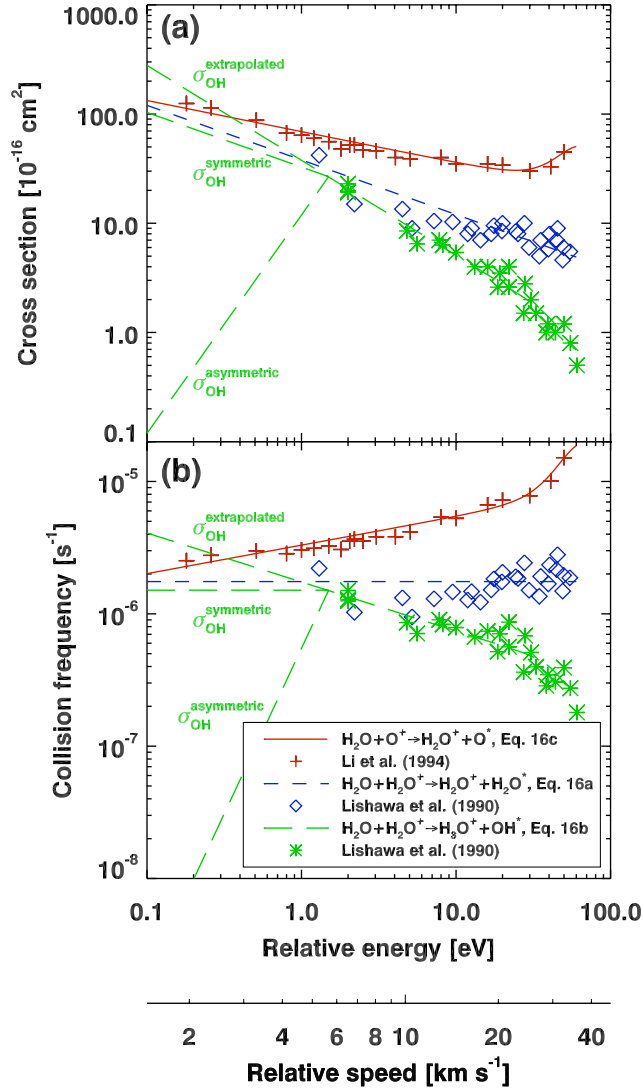


Figure 2. (a.) Cross sections for the reactions listed in the legend. Data for reactions 3a and 3b are from *Lishawa et al.* [1990], and data for reaction 3c is from *Li et al.* [1995]. $\sigma_{\text{OH}}^{\text{extrapolated}}$, $\sigma_{\text{OH}}^{\text{symmetric}}$, and $\sigma_{\text{OH}}^{\text{asymmetric}}$ are hypothetical fits applying to the OH*-producing reaction, and are explored in Fig. 4. Ions oscillate between ≈ 0 and 36 km s^{-1} in the Enceladus torus. (b.) Collision frequency, $n\sigma(v)v$, for a given density of $n_{\text{H}_2\text{O}} = 10^3 \text{ cm}^{-3}$ plotted over the same energy range. The collision frequency increases with energy in the oxygen-forming reaction, while the water-forming reaction is independent of energy and the OH-forming reaction declines with energy.

Charge exchange products by species

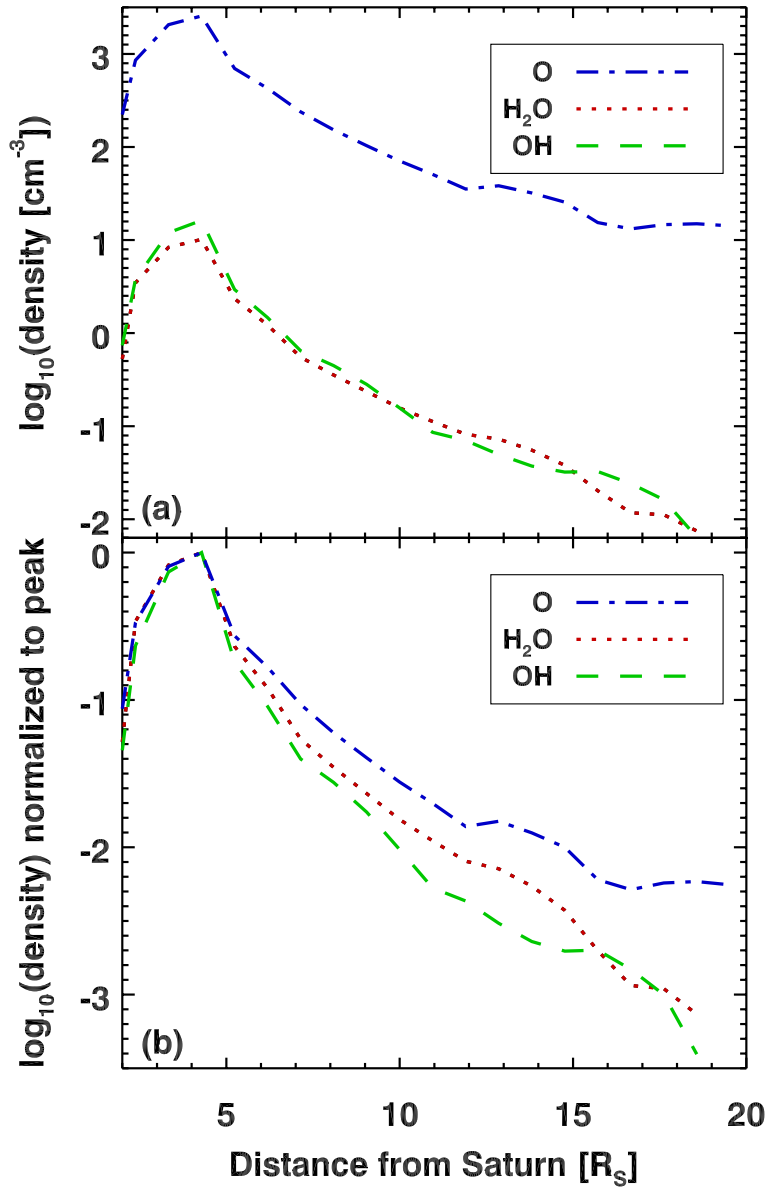


Figure 3. Neutral clouds produced by the reactions shown in Fig. 2. (a.) Oxygen is the most abundant because the cross section is $10\times$ higher than with O and OH. The lifetime of oxygen against photoionization is also much longer than the lifetime for either OH or H_2O against photodissociation. (b.) Same as above, but normalized to peak. Oxygen shows the most spreading because reactants are produced with higher velocities (Fig. 2b), which expands the cloud. The same trend holds with H_2O and OH, where OH tends to be created with the lowest velocities (Fig. 2, $\sigma_{\text{OH}}^{\text{extrapolated}}$).

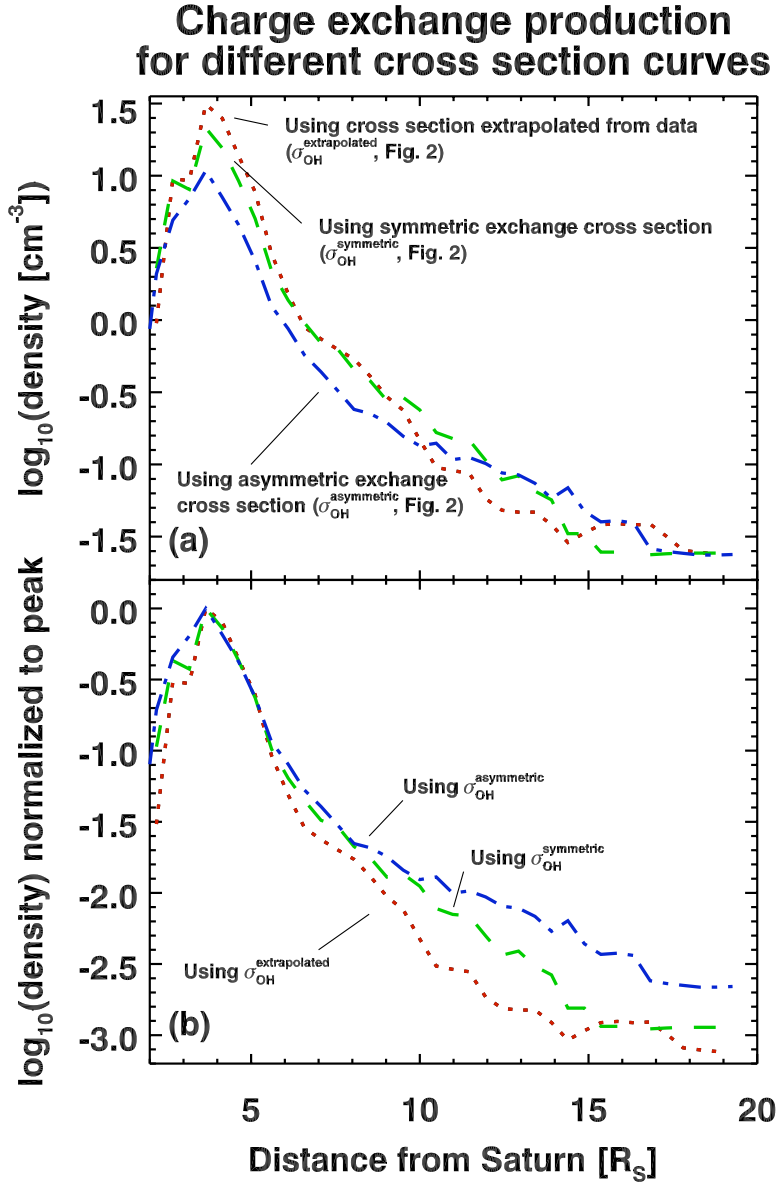


Figure 4. Neutral OH clouds produced from three hypothetical charge exchange cross sections:

$\sigma_{OH}^{extrapolated}$, $\sigma_{OH}^{symmetric}$, and $\sigma_{OH}^{asymmetric}$ (Fig. 2). (a.) $\sigma_{OH}^{extrapolated}$ produces the highest density

($\sigma_{OH}^{asymmetric}$, the lowest) at Enceladus because of the creation of additional low-velocity particles.

(b.) Same as above, but normalized to peak. The differences in density in the tail is not an indication of spreading, but rather further illustrates the deficiency in the peak density, going

from $\sigma_{OH}^{extrapolated}$ to $\sigma_{OH}^{asymmetric}$.

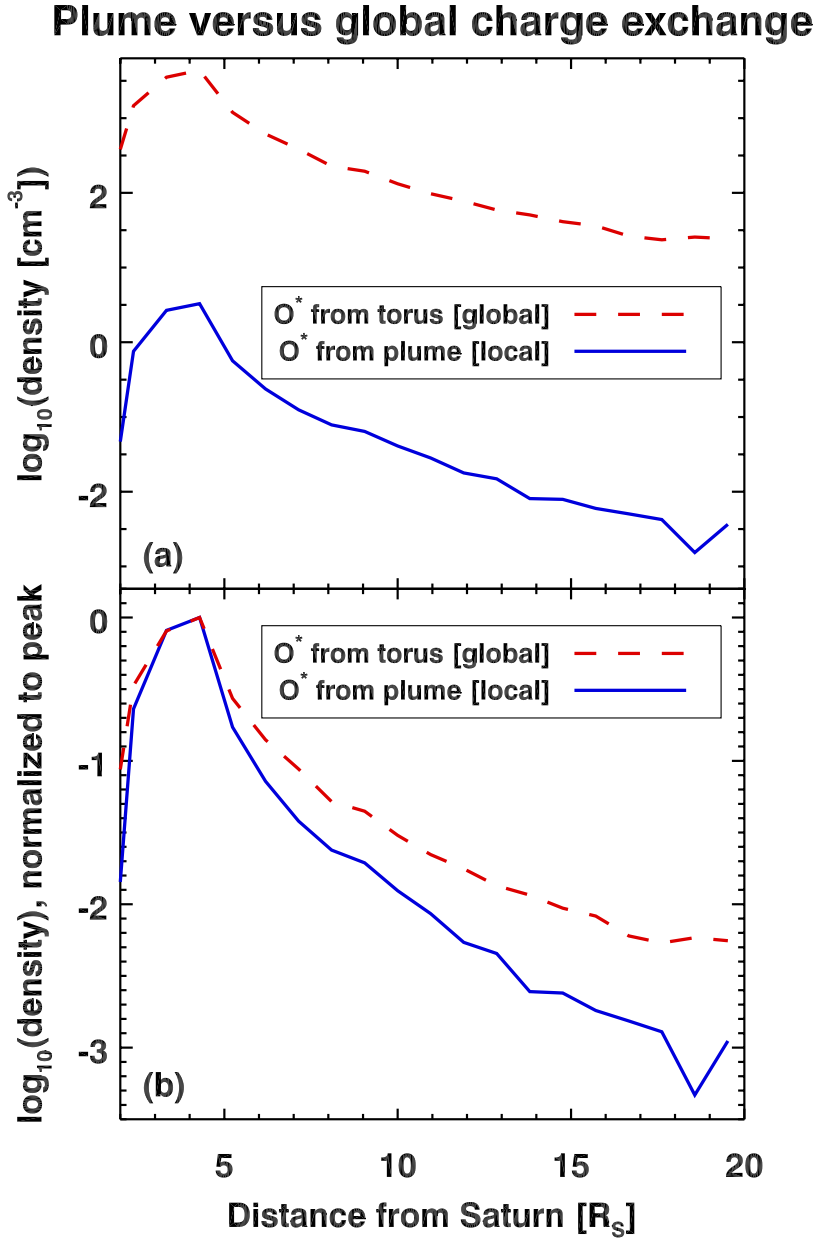


Figure 5. (a) Comparison between charge exchanged neutrals produced near the Enceladus plume and those produced from the neutral torus as a whole—in this case for oxygen. (b.) Though shown here for oxygen, all charge exchange reactions near the plume result in a cloud with less spreading than their global counterpart due to the imposed slowing of the plasma (and hence, the release of slower neutral products) near the plume in response to mass-loading [*Fleshman et al.*, 2010a].

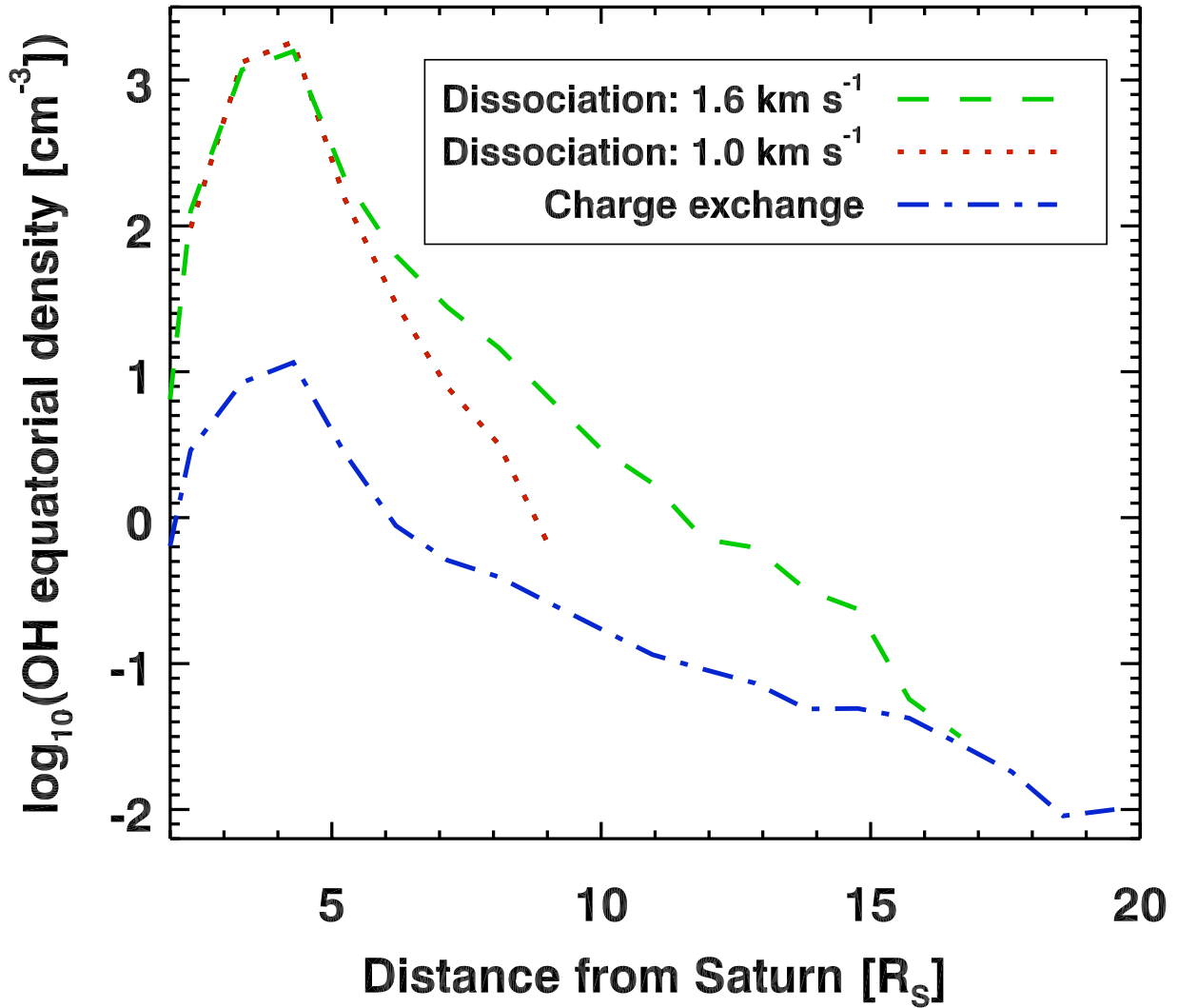


Figure 6. OH clouds produced from charge exchange and high- and low-speed dissociation. Dissociation dominates neutral cloud production inside 9–15 R_S, at which point charge exchange becomes the dominant contributor.

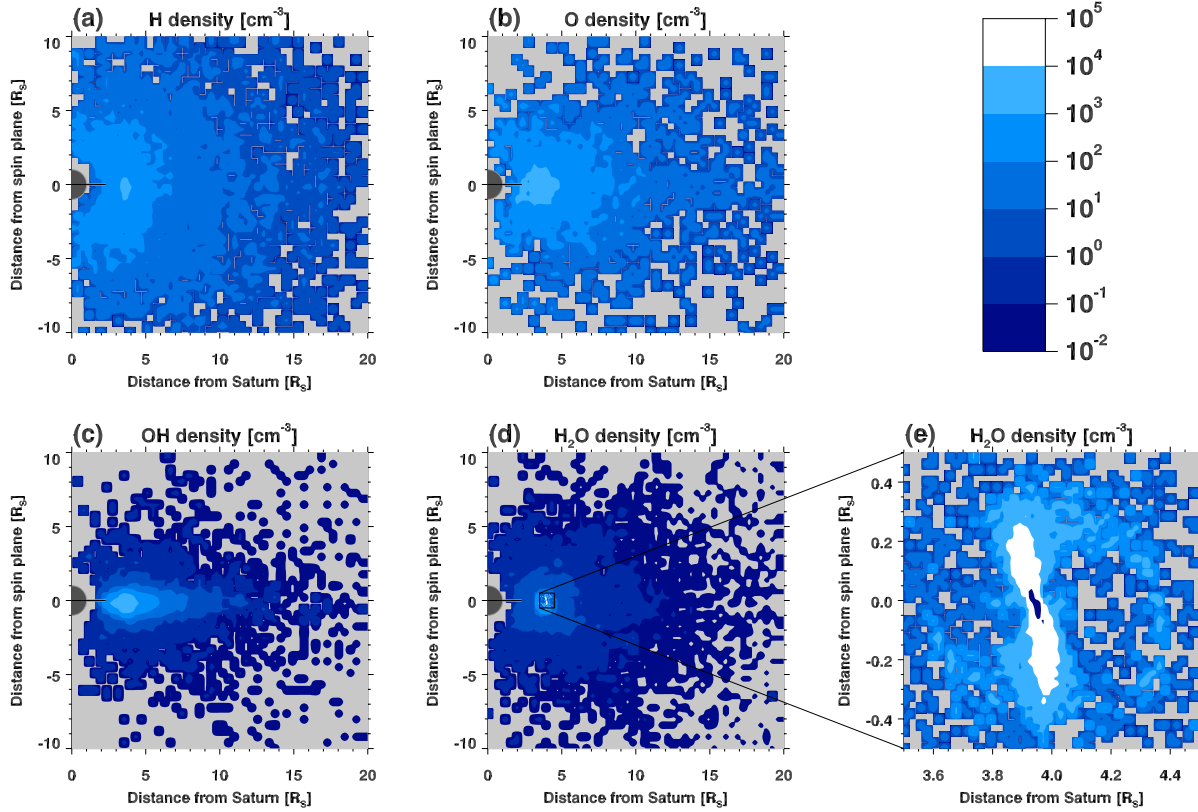


Figure 7. Neutral cloud densities in the r - z plane. (a.) Hydrogen produced purely from H_2O dissociation. (b.) Oxygen produced purely from charge exchange (reaction 3c). (c.) Hydroxyl produced from the combination of charge exchange and dissociation. Dissociation dominates inward of 9 – $15 R_S$ along the equator, while charge exchange (reaction 3b) tenuously fills the magnetosphere elsewhere. (d.) Water produced entirely by charge exchange (reaction 3a). (e.) Dense torus fed directly by the Enceladus plumes (section 2.1.2).

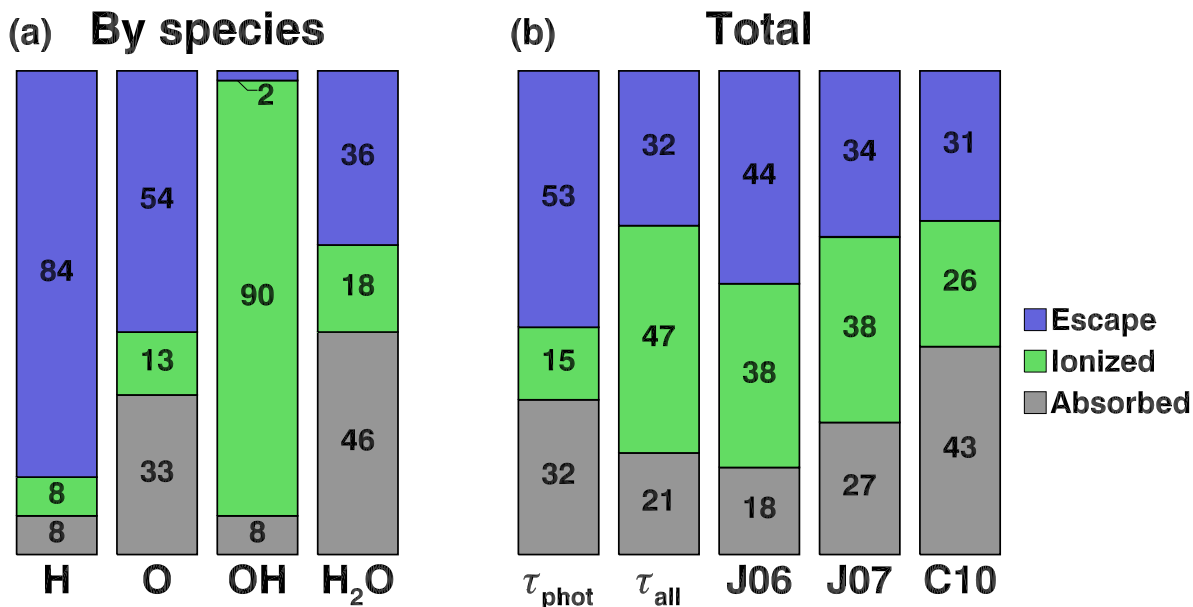


Figure 8. The fates of neutrals in our model along with the results from other models. (a.) Dissociation produces low-velocity neutrals and OH is thus not likely to escape or to be absorbed. Conversely, dissociation also produces hydrogen which largely leaves the system. (b.) The results of J06 [Johnson *et al.*, 2006], J07 [Jurac and Richardson, 2007], and C10 [Cassidy and Johnson, 2010], along with our own weighted totals (excluding hydrogen; see section 3.3.1). In the case of τ_{phot} , the lifetime of the cloud is determined by photoionization/dissociation only, whereas with τ_{all} , we limit the lifetimes by also including electron impact and charge exchange. These limiting cases bound the previous studies, except that C10 has more absorption attributed to neutral–neutral collisions.

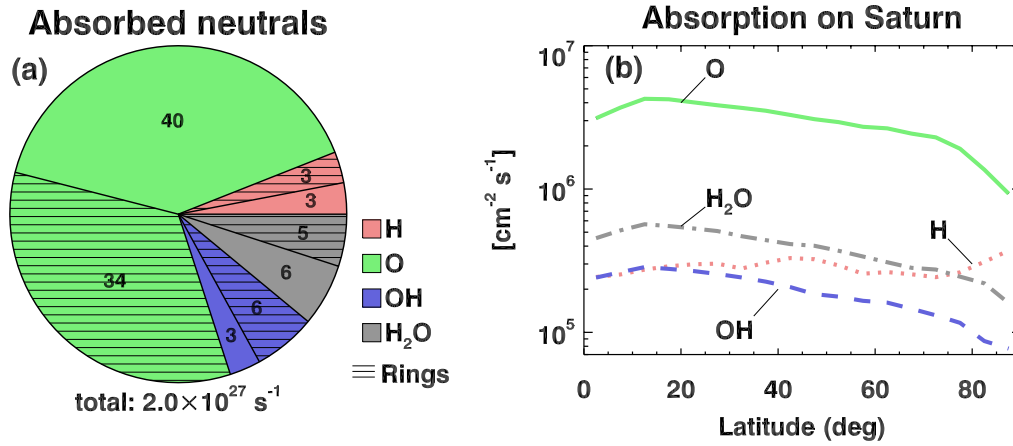


Figure 9. (a.) Neutrals absorbed by Saturn, plotted by species. Partitions with horizontal lines indicate percentages absorbed by Saturn’s rings. (b.) Neutral flux on Saturn as a function of latitude. Neutrals produced by charge exchange (H₂O, OH, and O) peak in flux at low latitudes due to the nature of the ion distributions from which they originate, which have initial velocity vectors predominantly in the ring plane. Conversely, hydrogen flux is constant across Saturn because it originates from dissociation, whose velocity distribution is prescribed as isotropic. Note that OH produced by dissociation is not energetic enough to reach Saturn.

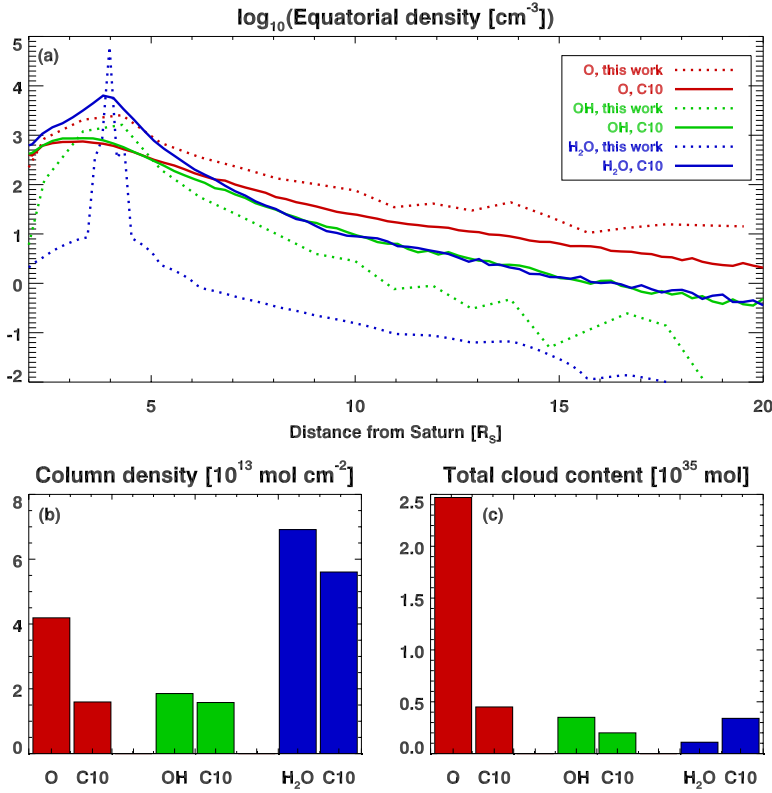


Figure 10. (a.) Total neutral clouds from our model, compared with *Cassidy and Johnson* [2010] (C10). All clouds include contributions from charge exchange (reactions 3a–3c), while H₂O is largely comprised of water sourced directly from Enceladus, and OH includes contributions from dissociation. The cloud densities are limited by photodissociation for OH and H₂O and by photoionization for O. Including charge exchange as a loss for cloud neutrals would reduce the lifetime for O more than for either the OH or H₂O, and would lower the relative oxygen abundance accordingly. (b.) Equatorial column densities found by integrating the plotted equatorial densities. The H₂O column density is similar to C10, despite their having a very different radial distributions. (c.) Total neutral cloud content. Our total H₂O content is less than C10 found, while our H₂O column density is higher because our H₂O cloud is not subjected to neutral collisions and is thus more confined.